Thesis for the degree of Licentiate of Engineering

Physics-based Modelling for Aircraft Noise and Emission Predictions

Evangelia Maria Thoma

Department of Mechanics and Maritime Sciences
CHALMERS UNIVERSITY OF TECHNOLOGY
Göteborg, Sweden 2022

Physics-based Modelling for Aircraft Noise and Emission Predictions
Evangelia Maria Thoma

Licentiatavhandlingar vid Chalmers tekniska högskola
Technical report No. 2022:05
ISSN 1652-8565

Department of Mechanics and Maritime Sciences
Chalmers University of Technology
SE–412 96 Göteborg, Sweden
Telephone + 46 (0) 31 – 772 1000

Chalmers Reproservice
Göteborg, Sweden 2022

Abstract

Physics-based Modelling for Aircraft Noise and Emission Predictions
Evangelia Maria Thoma
Department of Mechanics and Maritime Sciences
Division of Fluid Dynamics
Chalmers University of Technology

Starting from semi-empirical noise source models for the aircraft and 4D trajectory computations, this work focuses on the environmental assessment of scenario studies regarding technology evaluation and procedural planning. Extensive work was performed on improving and validating the existing tools. The physics based dynamic modelling for straight inflight was extended to account for a third space dimension and the inclusion of non-zero wind. Real flight data were used for model verification. Ground noise measurements were used to validate the physics-based prediction of source noise for varying operating conditions and to adapt the model to a state-of-the-art aircraft and engine. In this thesis, a summary of the developed physics-based methods and their validation are presented and the selected case studies are described.

An important part of the presented research focused on sustainability aspects and the evaluation of interdependencies between noise, NO_x and CO_2 emissions. New propulsion system designs were generated for a state-of-the-art ultra-high bypass ratio turbofan engine by allowing variation in the OPR (Overall Pressure Ratio), FPR (Fan Pressure Ratio) and BPR (Bypass Ratio). By varying these parameters, the engine was optimized for minimum installed specific fuel consumption. Allowing minimum fuel burn variation around this optimal point, different engine designs and operational characteristics were established and trades between LTO (Landing and Take-off) NO_x emissions and cumulative noise were examined.

Another aspect focusing on the sustainability of air transport concerns the operational level, where the aim is to establish improved procedures and trajectories through the use of the existing technology. Several noise abatement procedures already exist and are implemented to reduce pollution around airports. Focusing on approach procedures, these standard operations were evaluated for noise and emissions. More advanced procedures were designed and assessed for their environmental impact and optimization was carried out to establish the optimal procedure for specific cases. It was demonstrated that quantifying these trade-offs and adapting the design to specific conditions is essential when new flight procedures are designed.

Keywords: aircraft noise, emissions, physics-based modelling, FDR, measurements, interdependencies, turbofan engine, trajectories.

Acknowledgments

This research work was carried out at the Division of Fluid Dynamics, Department of Mechanics and Maritime Sciences at Chalmers University of Technology during 2020-2022. It is part of the CIDER project which is a cooperation between Chalmers University of Technology, Aurskall Akustik AB, Novair and KTH Royal Institute of Technology. The project is funded by the CSA (Centre for Sustainable Aviation) at KTH Royal Institute of Technology, Stockholm, Sweden in cooperation with the Swedish Transport Administration, Trafikverket.

Firstly, I would like to express my gratitude to my supervisors. Professor Tomas Grönstedt for giving me the opportunity to be a part of this project and pursue my PhD, as well as for his support, constant guidance and the many fruitful discussions. Doctor Xin Zhao for always finding the time for interesting discussions and constructive feedback and for his invaluable support, especially regarding the various tools and codes. Associate Professor Evelyn Otero Sola, from KTH, who even though she joined the project later, her constant guidance, knowledge and enthusiasm have been a great addition. I would also like to thank Ulf Tengzelius, from Aurskall Akustik AB, for the many interesting discussions and his advice and help regarding the noise modelling and the SAFT tool. Furthermore, I would like to express my gratitude to Henrik Ekstrand and Ulrika Ziverts, from Novair, not only for the input they have provided but also for their advice and for always finding the time for discussion. I am also grateful for the help I have received from several people at the CSA. My former supervisor Professor Mats Åbom for his guidance at the start of the project and his support on acoustics and Anders Johansson and Associate Professor Karl Bolin for performing the noise measurements and sharing the data.

I would also like to thank my colleagues at the Division of Fluid Dynamics and the Turbomachinery Group for creating such a nice working environment.

Finally, I would like to express my deepest gratitude to my family for their patience, love and support and my lovely friends, especially, Nikoletta for being an amazing friend and for always being there for me and Ioli who welcomed me here and has been a supportive and awesome friend since.

Evangelia Maria Thoma
Göteborg, May 2022

List of Publications

This thesis is based on the following appended papers:

Paper 1. Evangelia Maria Thoma, Tomas Grönstedt, Xin Zhao *Quantifying the Environmental Design Trades for a State-of-the-Art Turbofan Engine.* Aerospace 2020, 7, 148. https://doi.org/10.3390/aerospace7100148

Paper 2. Evangelia Maria Thoma, Tomas Grönstedt, Evelyn Otero, Xin Zhao. *Environmental Assessment of Noise Abatement Approach Trajectories.* 33rd ICAS Congress, September 4-9, 2022, Stockholm, Sweden. To be submitted

Nomenclature

AA	Air Attenuation
A_{EC}	Combustor exit area
AEDT	Aviation Environmental Design Tool
A_{Grd+RS}	Ground and refraction-scattering effects
ANOPP	Aircraft NOise Prediction Program
ANT	Approach Noise Trials
ATM	Air Traffic Management
BWB	Blended Wing Body
BPR	Bypass Ratio
C	Coherence coefficient
$\bar{c}$	Wing aerodynamic chord
c_0	Reference speed of sound
CDA	Continuous Descent Approach
C_{Dw}	Wing drag coefficient
CHOICE	CHalmers nOIse CodE
CIDER	CorrelatIon- and physics- based preDiction of noisE scenaRios
C_L	Speed of sound at the turbine exit
CP	Cycle Parameter
CSA	Center for Sustainable Aviation
c/s	Stator/rotor spacing
D	Drag
D_e	Combustor exhaust nozzle exit plane effective diameter / Equivalent diameter of the coaxial or circular jet
D_h	Combustor exhaust nozzle exit plane hydraulic diameter
$D(\theta)$	Directivity factor
DAC	Dual-Annular Combustor
E_{Eng}	Engine installation effect
EPNL	Effective Perceived Noise Level
f	Fuel flow (Chapter 2) / Frequency (Chapter 3)
f_0	Fundamental blade passage frequency of the last stage of the turbine
f_b	Fan blade passage frequency
F	Spectra
FAA	Federal Aviation Authority
FDR	Flight Data Recorders
FPR	Fan Pressure Ratio

G	Over-ground attenuation / Ground effects factor
GESTPAN	GEneral Stationary and Transient Propulsion ANalysis
ICAO	International Civil Aviation Organization
INM	Integrated Noise Model
L	Lift (Chapter 2) / Sound level (Chapter 3)
L_0	Peak sound pressure level for the turbine
L_c	Characteristic sound pressure level for the fan
L_C	Combustor nominal length
LDLP	Low Drag Low Power
L_{den}	Day - night yearly averaged sound pressure level
LTO	Landing and Take-Off
LG	Landing Gear
m	Aircraft mass
M	Mach number
M_{tr}	Rotor tip relative Mach number
M_{trd}	M_{tr} at fan design point
NADP	Noise Abatement Departure Procedure
N_f	Number of ignited fuel nozzles in the combustor
OAPWL	Overall Acoustic Power Level
OASPL	Overall Sound Pressure Level
OPR	Overall Pressure Ratio
P	Pressure
PANAM	Parametric Aircraft Noise Analysis Module
$\langle p^2 \rangle$	Mean square acoustic pressure
R	Turn radius (Chapter 2) / Distance between source and observer (Chapter 3)
RSL	Relative Spectrum Level
RSS	Rotor-Stator Spacing
SAC	Single-Annular Combustor
SAFT	Simulation of Atmosphere and air traFfic for a more silenT environment
S	Suppression factor
S_{dB}	Suppression in dB
SEL	Sound Exposure Level
SFC	Specific Fuel Consumption
SIL	Sound Intensity Level
S_l	Aggregated surface of the landing gear parts
SPL	Sound Pressure Level
S_w	Aircraft reference area
T	Thrust
TAS	True AirSpeed
TRA	Technology Reference Aircraft
T_0	Reference temperature
T_S	Static temperature
ULLA	Undersökningar medelst Ljudmätningar vid Landningar på Arlanda

V	True airspeed
V_e	Nozzle exit equivalent flow velocity
V_{GS}	Ground speed
V_{TR}	Relative tip speed of last rotor of the turbine
V_w	Wind speed
V_y	Vertical aircraft speed
W	Aircraft weight
W_3	Combustor inlet flow
WEICO	WEight and COst estimation
WHO	World Health Organization

Greek Symbols

α	Angle of attack (Chapter 2) / Absorption (Chapter 3)
β	Landing gear radiation efficiency
γ	Flight path angle
Δr	Path-length difference
ΔT	Temperature rise
η	Jet frequency parameter
θ	Pitch angle (Chapter 2) / Longitudinal directivity angle (Chapter 3)
Λ	Total lateral attenuation
ν	the kinematic viscocity
ξ	Angle between direction of aircraft and sound propagation path
ρ	Density
ϕ	Roll or bank angle (Chapter 2) / Lateral directivity angle (Chapter 3)
ϕ_w	Wind direction
ψ	Heading angle (Chapter 2) / Wing sweep angle (Chapter 3)

Subscripts

0	Reference value
3	Combustor inlet
4	Combustor exit
7	Turbine last stage
n	Normalized value
p	Peak value

Contents

Part I

Introductory Chapters

Chapter 1

Introduction

1.1 Background

One of the major detrimental effects of the aviation industry is noise pollution around the airports. Although it is, generally, linked with community annoyance, the most significant effect is its impact on human health which has been a topic of extensive discussion and research [3, 8, 15, 53]. Aircraft noise has been associated with sleep disturbance [36], increased risk for cardiovascular disease [11] and cognitive impairment [35], especially for children. It is also related to increased levels of stress and anxiety, which lead to mental health problems and poor productivity and performance [10].

According to the European Aviation Environmental Report 2019 [18], the total population exposed to L_{den} (day – night yearly averaged sound pressure level) above 55 dB, from aircraft at 47 major European airports, amounted to 2.58 million people in 2017. With the growth of air traffic, the exposure of people to aircraft noise is expected to increase. Despite the reduction in the number of flights due to Covid-19, it is expected that air traffic will reach the levels of 2019 by 2024 and grow by another 6% by 2027 [16]. Therefore, aircraft noise is still a major concern and efforts to reduce it have mostly been driven by ICAO guidelines [32].

The balanced approach proposed by ICAO recognizes four levels of aircraft noise mitigation [32]. These include noise reduction at the source (engine and airframe components), effective land-use planning and management, noise abatement operational procedures and restrictions of operations. Actions taken within any of these levels should be evaluated for their environmental impact. Even though noise does not have a direct impact on the climate, variations in procedures or in engine/aircraft design influence the production of CO_2 and NO_x emissions. It is therefore important to consider these interdependencies when low-noise solutions are examined.

1.2 Noise mitigation and interdependencies

Aircraft noise is a complex problem that can be analysed on many levels. Research on noise mitigation concepts has mostly focused either on the reduction at the source or on flight procedures improvement. The former concerns more long-term solutions but would require replacing existing fleets and potentially redesigning airport infrastructure. That would, for example, be the case for the BWB (Blended Wing Body) concept and possibly for the Box-Wing concept, both of which are described by Knobloch et al. [37], together with other novel designs. The latter, i.e. flight procedures improvement, can be directly applied to existing aircraft. Although advanced procedure design is a complex matter that requires accounting for operational constraints, safety limitations and balancing the needs of different stakeholders, such as airlines, airports, ATM (Air Traffic Management) operators and people affected by aircraft noise, it can lead to significant improvement, especially if adapted to specific conditions.

Reducing aircraft noise at the source requires identifying the dominating noise components. For take-off, the major noise source is the aircraft engine, with the fan and jet consisting of the dominant noise contributors. For approach and landing, the importance of the airframe noise increases while the fan still remains an important contributor. Engine noise has significantly improved with the introduction of high bypass ratio engines and the use of acoustic lining. An overview of the developed noise reduction technologies and the progress achieved in this area is presented by Liu et al. [44]. Further improvement can be achieved through engine design and cycle operation optimization [12, 22]. Cumpsty et al. have performed an extensive review on the environmental impact of aviation summarized in [12]. The review concerned four classes of subsonic aircraft and discussed the progress that has been achieved in terms of fuel efficiency and noise and emission reduction, relative to the goals being set by ICAO. Potential scenarios that could yield further improvement are assessed and new goals are proposed. Different aspects of air travel are considered and examined either separately or in relation to each other. A case where the engine OPR is varied is presented and the corresponding effect on LTO NO_x emissions is evaluated, indicating that NO_x emissions are highly dependent on combustor exit temperature and OPR. Fuel burn and noise are treated together and an optimization study is performed for several engine and aircraft parameters and for the four aircraft classes. The resulting Pareto fronts for the single aisle aircraft are presented in Figure 1.1. The TRA (Technology Reference Aircraft) is a 2017 model and 2027 and 2037 technologies are examined for three (high, nominal, low) confidence levels with respect to successful technology introduction. It is demonstrated that the optimal noise solution would result in the worst fuel burn scenario while the most fuel-efficient solution would cause high levels of noise. Hence a balanced approach with 50% weighting factor for each objective could be followed. Gliebe and Janardan [22] performed a system level study aiming in a 5 to 10 EPNdB community noise reduction. Four engine designs were evaluated for a large twin-engine civil aircraft. The same core technology was assumed for all the designs but FPR and BPR were allowed to vary. Additionally, two counter-rotating fan engine configurations were examined. They concluded that

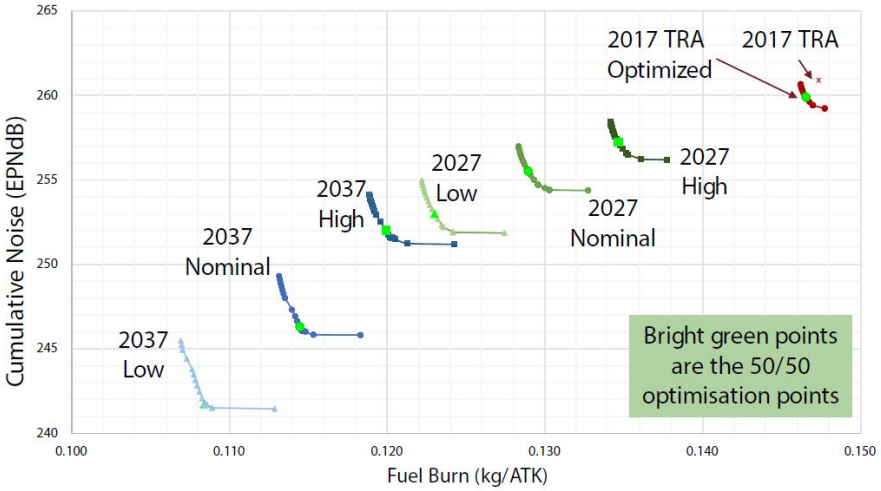

Figure 1.1: Pareto fronts for single aisle aircraft [12].

for FPR 1.5 or less, significant noise improvement can be achieved, while the counter-rotating fan engines also resulted in important noise reduction. A similar study was performed as part of the presented work and the relevant publication is appended at the end of the present thesis. A more detailed description regarding the study is presented in Section 4.1.

Regarding the airframe noise, the major contributors are the high-lift devices and the landing gear. Research in this area is mainly focused on developing new design concepts for these components, the whole aircraft or using noise reduction mechanisms such as acoustic liners and fairings. A review of the major findings in airframe noise reductions is presented by Yong et al. [60]. The review is mostly focused on passive control methods, such as fairings, slat cover, edge replacements and other noise suppression technology but more advanced low-noise aircraft design concepts are also discussed. It is indicated that these concepts require careful assessment to account for safety and in order to avoid significantly affecting the performance of the aircraft.

The other aspect of noise reduction is concerned with noise abatement procedures and trajectory optimization. Both for the case of departure and approach, there are some standard operations that can be implemented to reduce noise, namely the noise abatement procedures. For departure, there are mainly two procedures: NADP 1 and NADP 2 (NADP: Noise Abatement Departure Procedure), introduced by ICAO [34]. NADP 1 is designed to reduce noise directly underneath the flight path and close to the airport, while NADP 2 mitigates noise further out along the flight path. The main actions involved in these procedures are power reduction and variation in the flap/slat retraction altitude. For approach, the most common procedures are the CDA (Continuous Descent Approach) [33] and the LDLP (Low Drag Low Power) [9]. These include actions such as increased flight altitude for the former and lower power requirement and delayed configuration changes for the latter. Other possibilities to manage approach noise include steeper approach angle and displaced landing threshold [20]. Most studies in this area focus on trajectory optimization. Zhang

et al. [63] performed state parametrization using Bézier approximation curve and optimized the 4D departure trajectory for noise minimization and CO_2 emissions, using Genetic Algorithm and Particle Swarm Optimization. It was shown that a lower target speed for the initial acceleration part and constant speed climb to 3000 ft could result in noise reduction, while for altitude higher than 3000 ft the lower speed impact on noise is not so significant but could contribute to lower emission production. Another conclusion was that a detour, with the appropriate speed and within a specified flying range, could be implemented in some cases to avoid high ground noise level. Visser et al. [57] proposed a generalized tool for the assessment and development of noise abatement procedures with a focus on departure procedures. The tool was tested for a departure route to generate fuel minimum and noise minimum trajectories. It was shown that noise reduction in the proximity of the runway is traded with increased noise level further away. The fuel optimal trajectory implemented a full thrust low altitude horizontal turn which caused an increase in noise level. It was indicated that the thrust cutback was the main action in order to reduce noise in specific areas. Finally, it was shown that allowing more freedom to the design parameters resulted in further improvement in fuel consumption but not so much in noise reduction. Koenig and Macke [38] evaluated several noise abatement approach procedures with respect to noise and pilot workload. They concluded that the introduced more advanced procedures lead to a greater noise reduction than the reference LDLP trajectory. However, there are other aspects to consider such as feasibility and economical aspects. The best option seemed to be a segmented CDA, even though it caused increased pilot workload and raised some safety concerns. It is stated that further work should be performed in this area. Zhang and Filippone [62] performed a segmented optimization for arrival flight for minimum environmental impact, looking both at a single aircraft and at a fleet of four aircraft. They determined that the lowest noise level solution does not always correspond to the lowest number of awakenings and that the optimal CO_2 solution is not necessarily associated with the shortest operation. It becomes apparent that research in this area is rather active. In Section 4.2, a study where several approach trajectories are assessed for their environmental impact is also presented.

1.3 Noise prediction

Aircraft noise prediction methods can generally be classified into two categories: the integrated or best practice methods and the simulation based or theoretical methods. The more commonly used methods and tools, i.e. the ECACdoc29 [17] and the FAA's (Federal Aviation Authority) INM (Integrated Noise Model) [5] and AEDT (Aviation Environmental Design Tool) [19], fall into the first category. These methods are based on databases and consider the aircraft as a whole. They are able to provide a good estimation for long-term averages and are used by several airports and national authorities. However, they do not provide any information about the individual component contribution to the total noise. The second category of noise prediction tools includes the physics-based and the correlation-based prediction. For

the correlation-based prediction, a noise source model is developed from back-propagated ground noise measurements and real flight data for a given aircraft type. Such a model was presented by Zellmann et al. [61]. The physics-based prediction assumes that the total aircraft source noise can be estimated by modelling and summing all the individual noise components at the same frequency. It is common to refer to noise source models developed in this way as semi-empirical. The most widely known tools in this category are ANOPP (Aircraft NOise Prediction Program) [64] and PANAM (Parametric Aircraft Noise Analysis Module) [4]. The drawback of these tools is that they are not publicly available. A detailed description on the existing tools and methods in aircraft noise prediction can be found in the extensive review regarding aircraft noise prediction presented by Filippone [20].

In this work, an aircraft noise prediction tool that falls in the category of physics-based methods will be presented. It was developed based on empirical and semi-empirical sound source models found in public literature. Most of these models are common to the ones implemented in ANOPP or ANOPP2. The total SPL (Sound Pressure Level) is computed for every frequency and longitudinal directivity as the sum of the individual components for every point along a given trajectory. Flight effects such as atmospheric attenuation, spherical spreading, Doppler shift, ground reflection, lateral attenuation and retarded time, are then included and the SPL matrix at the microphone is estimated. This is then converted to EPNL (Effective Perceived Noise Level) in order to allow for comparison with the standard certification procedure. A basic outline of the model is presented in Figure 1.2 and a more detailed description is provided in Chapter 3.

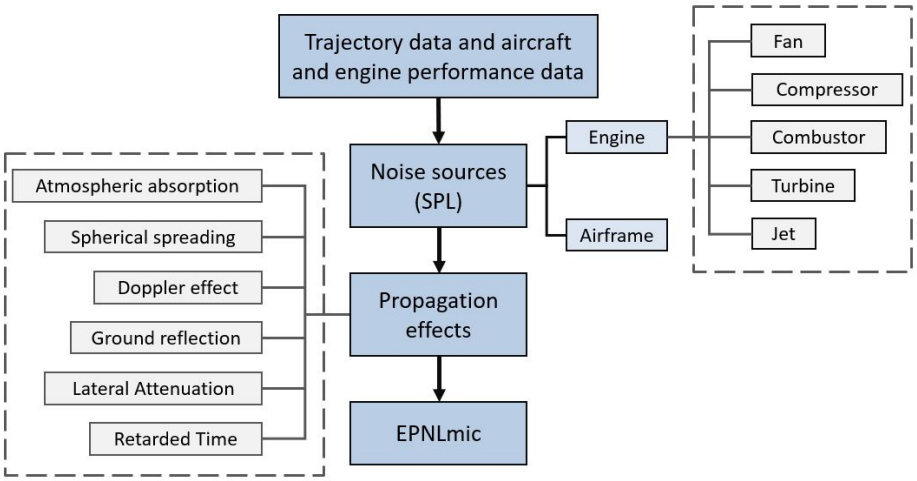

Figure 1.2: Outline of the physics-based model.

1.4 CIDER project

The work presented in this thesis is part of the CIDER (CorrelatIon- and physics-based preDiction of noisE scenaRios) project [7], which is run within the CSA (Centre for Sustainable Aviation). The project outline is depicted in Figure 1.3. It is run

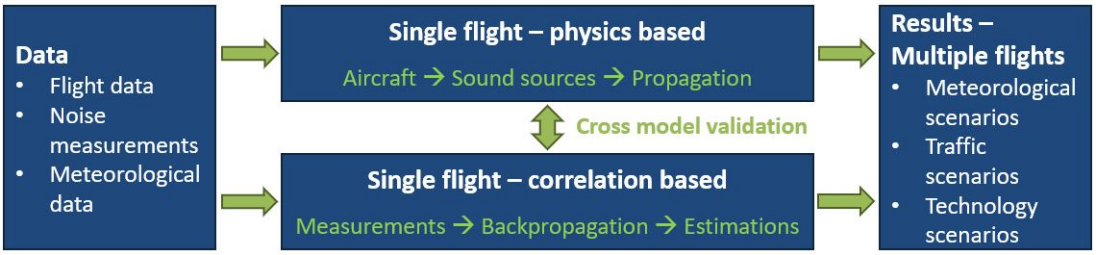

Figure 1.3: CIDER project scope.

in two parallel efforts, the physics–based prediction of noise, which is the focus of this work, and the correlation–based prediction. Both processes start from data collection and processing which are then used to develop and validate the models. These data include FDR (Flight Data Recorder) data provided by Novair [46] and corresponding ground noise measurements from the ULLA (Undersökningar medelst Ljudmätningar vid Landningar på Arlanda) project [55], as well as meteorological data. The developed models are then applied to study different scenarios, such as evaluation of different engine designs and trajectory optimization for low noise solutions.

1.5 Thesis outline and objectives

The progress that has been achieved within the first modelling effort will be presented in the following chapters. Starting from the aircraft performance, the 3D (two space dimensions and time) flight dynamics model was extended to allow for computing curved flights (4D) and the inclusion of non-zero wind. FDR data from selected flights were used for the model validation. A detailed description of the model development and validation is provided in Chapter 2. For the engine performance and conceptual design, already existing and verified tools developed at Chalmers were used, namely GESTPAN (GEneral Stationary and Transient Propulsion ANalysis) [27] and WEICO (WEight and COst estimation) [28]. Work was only performed to develop a model for the A321neo with Leap-1A engine. The noise source models were already in place in the noise prediction tool CHOICE (Chalmers nOIse Code) [14]. Its basic outline was already depicted in Figure 1.2. Some modifications were made to the original code which was then validated using the available noise measurements. A connection with the noise mapping tool SAFT (Simulation of Atmosphere and air traFfic for a more silenT environment) [51] was also established in order to generate contours of the ground noise level underneath a given trajectory. The aim of the present work and project is to define and perform scenario studies using the developed models. Two of the selected studies are presented in this thesis.

Chapter 2

4D Trajectory Model

The prediction of the environmental impact of any scenario starts from the trajectory and performance modelling of the aircraft. The development of an accurate trajectory model is, therefore, a necessary first step. For this reason, the physics-based flight dynamics model was extended to allow for the simulation of curved flights and to account for the effect of the wind. The extended model includes another degree of freedom for the relative wind and two additional states in the integration method of the key aircraft performance equations. Development and verification of the model was performed using FDR data for the A321neo but the dynamic equations are applicable for any aircraft. The focus of the analysis will mainly be on the approach phase of the flight as this was the key focus of the CIDER project.

2.1 Data availability and processing

The models developed in this work concern the A321neo with the Leap-1A engine. The aircraft is a narrow-body jet-airliner produced by Airbus that entered into service in May 2017. The engine is a two shaft direct drive turbofan with high BPR.

The available FDR data were provided by Novair. They included the entire mission for a hundred flights during the period from 2019-05-04 to 2019-09-15 with Arlanda airport in Stockholm as the destination. From the data only the approach phase of the flight was selected and a down-selection of the available parameters was used for the model development and verification. These parameters included trajectory details (aircraft position and altitude), Mach number, vertical speed, static temperature, flap and slat setting, pitch and roll angle, wind speed and wind direction. It was then possible to determine the true airspeed, the flight path angle and the angle of attack using the following equations

$$V = c_0 M \sqrt{\frac{T_s}{T_0}} \tag{2.1}$$

$$\gamma = \arcsin\left(\frac{V_y}{V}\right) \tag{2.2}$$

$$\alpha = \theta - \gamma \tag{2.3}$$

where c_0 is the reference speed of sound and T_0 the reference temperature, equal to 340.29 m/s and 288.15 K, respectively. M is the mach number, T_0 the static temperature, V_y the vertical speed and θ the pitch angle.

Regarding the aerodynamic characteristics of the aircraft, there were no available data in the FDR data set. Thus, a model for the A321-231 had to be set up to estimate the lift-to-drag ratio for the different configurations (flap and slat setting) and landing gear positions assuming that the ratio between the two aircraft types remains the same. The configuration settings and the respective lift-to-drag ratio are presented in Table 2.1. Two columns are shown for the ratio values corresponding to landing gear retracted (w.o. LG - without landing gear) and extended (w. LG - with landing gear). Landing is usually performed with configuration 3 or FULL, while configuration 1+F is mainly used during take-off.

Configuration	Slats (^{o})	Flaps (^{o})	L/D w.o. LG	L/D w. LG
0	0	0	17.76	-
1	18	0	15.38	-
1+F	18	10	13.17	-
2	22	14	12.45	9.35
3	22	21	10.96	8.88
FULL	27	35	-	8.32

Table 2.1: Configurations and estimated lift-to-drag ratio for A321neo.

2.2 Curved flight

2.2.1 Turning performance

Turning the aircraft is achieved in the same way as climbing, i.e. by using the lift force. Lift is mainly generated by the wings and in a straight flight it is pointing upwards, perpendicular to the flight path. In order for the aircraft to turn, it needs to be banked, generating a horizontal component of lift towards the center of the turn. This horizontal component is also referred as the centripetal force, Figure 2.1.

The simplest case is that of an aircraft in level turn, as presented in Figure 2.1, during which the aircraft is turning while in level flight. In this case the vertical component of lift must be equal to the weight of the aircraft, W, since no other force is acting perpendicular to the flight path in the vertical plane, assuming a zero angle of attack. Hence, the following equations apply

$$\begin{cases} L\cos(\phi) = W \\ L\sin(\phi) = m\frac{V^2}{R} \end{cases} \tag{2.4}$$

where ϕ is the bank or roll angle, R is the turn radius and $V^2/R = a_c$ is the centripetal acceleration, which is directed radially towards the center of rotation – the center of the instantaneous circle. From the above equations, one can easily compute the

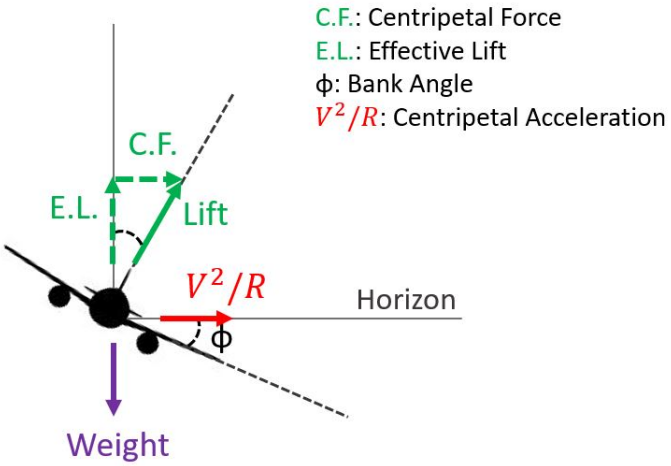

Figure 2.1: Free body diagram of an aircraft in banked turn.

radius of turn from eq. 2.5. This is a good approximation that can also be found in pilots' handbooks. However, it concerns the ideal case of level turn. This is rarely the case as usually the pilot has to perform a climbing or descending turn in non-zero wind conditions. These cases will be analysed in the next section.

$$R = m\frac{V^2}{g\tan\phi} \tag{2.5}$$

2.2.2 Equations of motion

The derivation of the dynamic equations describing the motion of the aircraft in three dimensions can be found in many flight mechanics books such as [45]. The general assumption is that all forces are acting on the center of mass of the aircraft and the velocity vector is considered in the plane of symmetry of the airplane, i.e. the sideslip angle is zero. The equations of motion for a flight over a flat earth are then given by

$$\begin{cases} T\cos(\alpha) - D - W\sin(\gamma) = m\dot{V} \\ (T\sin(\alpha) + L)\cos(\phi) - W\cos(\gamma) = mV\dot{\gamma} \\ (T\sin(\alpha) + L)\sin(\phi) = mV\cos(\gamma)\dot{\psi} \\ \dot{x} = V\cos(\gamma)\cos(\psi) \\ \dot{y} = V\sin(\gamma) \\ \dot{x} = V\cos(\gamma)\sin(\psi) \\ \dot{W} = -f \end{cases} \tag{2.6}$$

where T is the thrust for the total number of engines, α the angle of attack, D the drag, ψ the heading or yaw angle and f the fuel consumption.

The first three equations in eq. 2.6 are derived based on the body axis system (x'-y'-z') and the rest based on the ground system (x-y-z) presented in Figure 2.2. These

definitions are slightly different from the ones used by Miele [45]. The attitude angles γ, ϕ and ψ are also shown in the same figure.

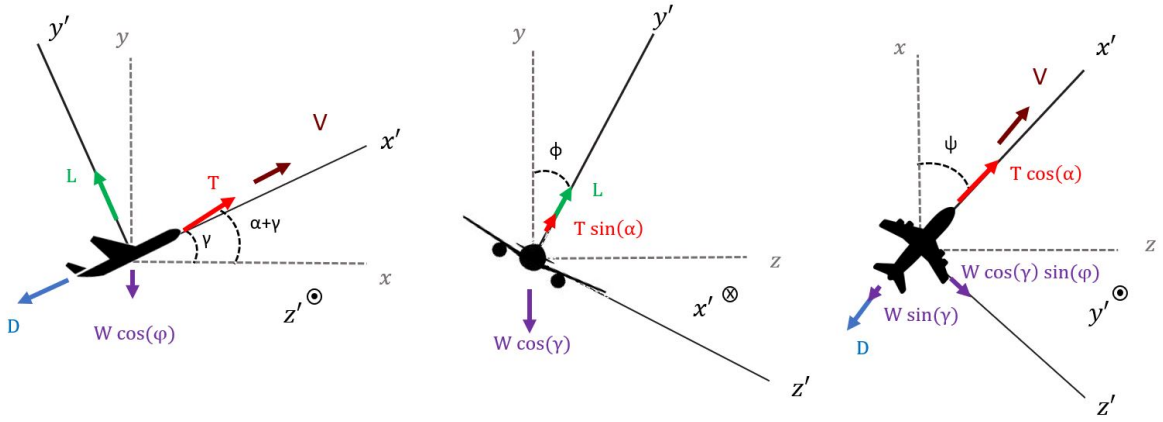

Figure 2.2: Coordinate system and aircraft free body diagram in three dimensions.

2.2.3 Equations of motion with wind

The movement of the aircraft and its trajectory while on the air are controlled using the control devices on the aircraft, e.g. ruder, slats, flaps etc. However, one key factor that can alter the aircraft's path is the wind. Wind speed and direction can have a significant effect on the flight, and it is important to consider them when planning routes.

When the aircraft is flying in crosswind conditions, it tends to deviate from its actual or desired path. This deviation is called drift and is defined as the angle between the aircraft heading, the direction in which the nose of the aircraft is pointing, and its track, the direction in which the aircraft is actually going. In order to maintain the aircraft in the desired course, its heading must be corrected depending on the wind speed and direction. The angle that the aircraft must be turned is referred as wind correction angle. It is often assumed that the drift and the wind correction angle are equal. While in some cases this might be true, they are not the same angle by definition as explained by Alexander and Klose [2]. Finally, in the case that wind and aircraft have the same direction, the heading and the track coincide. This phenomenon is called tailwind, while the opposite is called headwind.

With the inclusion of wind, there are two velocity vectors that are used to describe the motion of the aircraft. The first is TAS (True Airspeed), which is the velocity of the aircraft relative to the air. In this thesis, true airspeed is symbolised with V and it can, generally, be derived from the Mach number according to eq. 2.1. The second velocity vector is GS (Ground Speed), which is defined as the velocity of the aircraft relative to the ground. Ground speed can be determined from true airspeed with a simple vector addition with the wind velocity, as indicated by eq. 2.7.

$$\overrightarrow{V}_{GS} = \overrightarrow{V} + \overrightarrow{V}_w \tag{2.7}$$

where the wind velocity is written relative to the ground axis system as

$$\overrightarrow{V}_w = V_{wx}\vec{i} + V_{wz}\vec{j} + V_{wy}\vec{k} \tag{2.8}$$

Wind speed and direction are provided in the FDR data. The provided wind direction is measured from true north, i.e. wind direction equal to 0^o corresponds to wind blowing from north to south. For the calculations and for the equations that will be presented it is adjusted and refers to the angle between the wind velocity vector and the true airspeed.

For the derivation of the three-dimensional dynamic equations of motion for the case of flight in wind, only horizontal wind was considered, but a vertical component can easily be incorporated. The equations of motion in this case are derived using the absolute acceleration of the aircraft relative to the ground.

$$\overrightarrow{F} = m\overrightarrow{\dot{V}_{GS}} = m\left(\overrightarrow{\dot{V}} + \overrightarrow{\dot{V}_w}\right) \tag{2.9}$$

The acceleration of the aircraft relative to the air from eq. 2.6 and Figure 2.2 is defined as

$$\overrightarrow{\dot{V}} = \dot{V}\vec{i'} + mV\dot{\gamma}\vec{j'} + mV\cos(\gamma)\dot{\psi}\vec{k'} \tag{2.10}$$

The acceleration of the wind, accounting only for the horizontal components, is derived from eq. 2.8 as

$$\overrightarrow{\dot{V}_w} = \dot{V}_{wx}\vec{i} + \dot{V}_{wz}\vec{j} + V_{wx}\frac{d\vec{i}}{dt} + V_{wz}\frac{d\vec{j}}{dt} \tag{2.11}$$

with $V_{wx} = V_w\cos(\psi + \phi_w)$ and $V_{wz} = V_w\sin(\psi + \phi_w)$

However, the ground axis system is always fixed relative to the earth and therefore invariable with time. Thus, eq. 2.11 becomes

$$\overrightarrow{\dot{V}_w} = \dot{V}_{wx}\vec{i} + \dot{V}_{wz}\vec{j} \tag{2.12}$$

Using rotational matrices eq. 2.12 can be rewritten relative to the body axis system.

$$\begin{aligned}\overrightarrow{\dot{V}_w} = \left(\dot{V}_{wx}\cos(\psi) + \dot{V}_{wz}\sin(\psi)\right)\cos(\gamma)\vec{i'} - \left(\dot{V}_{wx}\cos(\psi) + \dot{V}_{wz}\sin(\psi)\right)\sin(\gamma)\vec{j'} \\ \left(-\dot{V}_{wx}\sin(\psi) + \dot{V}_{wz}\cos(\psi)\right)\vec{k'}\end{aligned} \tag{2.13}$$

Then, eq. 2.6 becomes

$$\begin{cases}\dot{V} = \frac{1}{m}\left(T\cos(\alpha) - D - W\sin(\gamma)\right) - \dot{V}_{wx'} \\ \dot{\gamma} = \frac{1}{mV}\left(\left(T\sin(\alpha) + L\right)\cos(\phi) - W\cos(\gamma)\right) - \frac{\dot{V}_{wy'}}{V} \\ \dot{\psi} = \frac{1}{mV\cos(\gamma)}\left(T\sin(\alpha) + L\right)\sin(\phi) - \frac{\dot{V}_{wz'}}{V\cos(\gamma)} \\ \dot{x} = V\cos(\gamma)\cos(\psi) + V_w\cos(\psi + \phi_w) \\ \dot{y} = V\sin(\gamma) \\ \dot{z} = V\cos(\gamma)\sin(\psi) + V_w\sin(\psi + \phi_w) \\ \dot{W} = -f\end{cases} \tag{2.14}$$

where $\dot{V}_{wx'}$, $\dot{V}_{wy'}$ and $\dot{V}_{wz'}$ are the components in eq. 2.13.

2.3 Model validation

Due to the lack of aerodynamic and engine performance data in the FDR the full model could not be directly validated. That means that it was not possible from the available data to integrate all the equations in eq. 2.14 and compute the flight path. Instead, the estimation of individual parameters was examined. Several flights from the data were used for the validation process but for brevity only one example is presented in the thesis.

The first two equations from eq. 2.14 were used, together with the lift-to-drag ratio values from Table 2.1, to estimate the lift, the drag and the thrust. The thrust estimation was compared with the engine rotational speed as indicated in Figure 2.3. As it would be expected, it is shown that the thrust correlates well with the engine rotational speed, i.e. when the engine throttles up the thrust goes up. This is a good indicator that both the lift-to-drag ratio and the thrust prediction can be used with rather good accuracy.

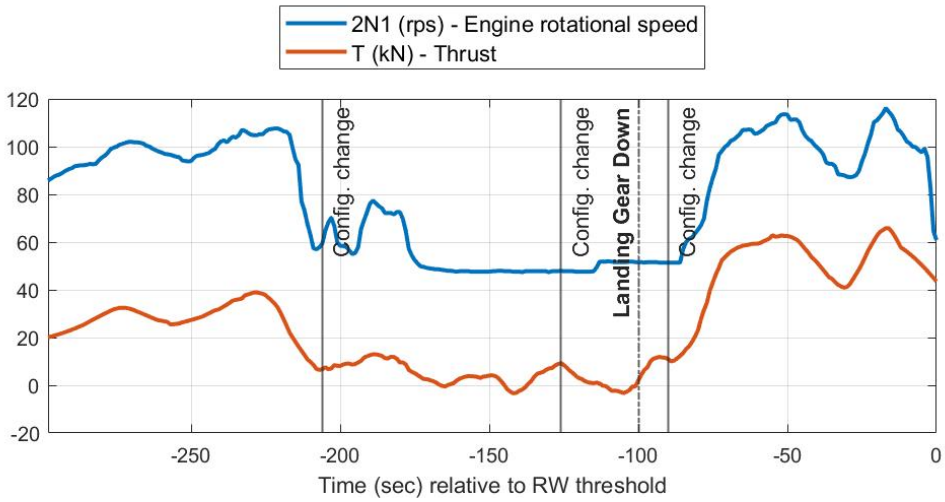

Figure 2.3: Thrust estimation compared to engine rotational speed data.

The thrust and lift estimation were used to estimate the rate of change of heading from the third equation in eq. 2.14. Then, $\dot{\psi}$, $\dot{x}$, $\dot{y}$, $\dot{z}$ and $\dot{W}$ were integrated to compute the heading and flight path of the aircraft which were then compared with the data. A summary of the required input parameters and the outputs from the model is presented in Table 2.2. The ground path Cartesian coordinates were converted to geographical coordinates using the Haversine formula which can be found in [56].

The heading angle from the integration is compared with the recorded in Figure 2.4. It is apparent that the two parameters match well. The difference between the two curves remains below 3^o for all the points. One thing that should be noted is that the heading angle in the data is recorded with respect to the magnetic north. That means that it varies from the true heading depending on the location of the aircraft and it should, therefore, be corrected accordingly. Since all the available flights have

the Arlanda airport in Stockholm as the destination and only the final approach phase is studied here, the heading can be corrected by accounting for the magnetic variation of Arlanda which is equal to 6^o to the East [52].

Inputs	Source	Outputs
V	eq. 2.1 with M, T_s from FDR	T
γ	eq. 2.2 with V_y from FDR	D
α	eq. 2.3 with θ from FDR	L
V_w	FDR	ψ
ϕ_w	FDR	x
L/D	Model	y
f	FDR	z
		W

Table 2.2: Summary of inputs and outputs to the model.

The estimated path from the integration is presented in Figure 2.5 and Figure 2.6, in three and two dimensions, respectively. The computed path is very close to the real one, with a final point deviation of 0.1 km in horizontal distance and only 1.2 m in altitude. The maximum deviation that occurs along the ground path is 0.5 km, while the maximum deviation in altitude amounts to 10 m. These values are considered acceptable. Apart from the model, some deviations may occur due to inaccuracies in the data. The attitude indicator is one of the most common sources of inaccuracies in FDR data. For example, it is not unusual that when the aircraft returns to straight flight after a steep turn the attitude indicator will show a slight turn towards the opposite direction of the performed turn. This can result in errors of about 3^o to 5^o that are corrected by internal mechanisms within a few seconds. Finally, one should also consider possible errors from the geographical coordinates conversion formula which can yield up to 0.3 % deviation [56].

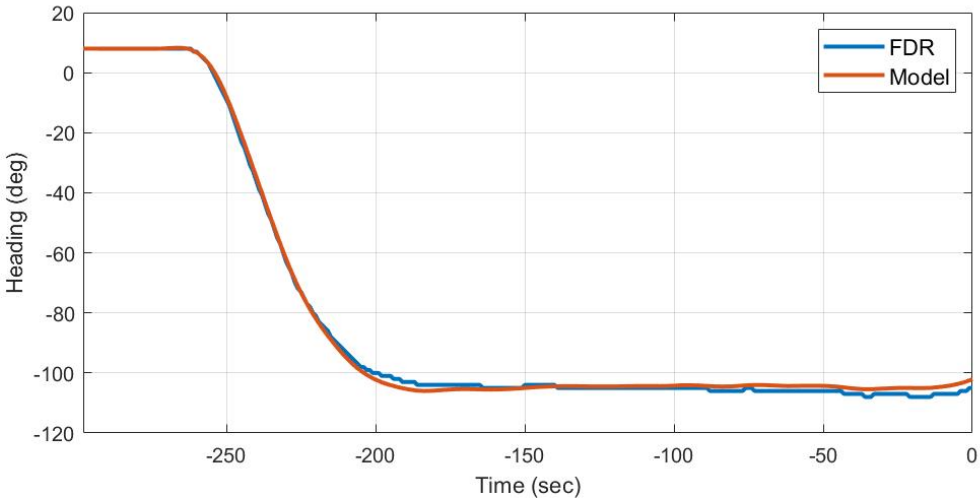

Figure 2.4: Heading angle comparison.

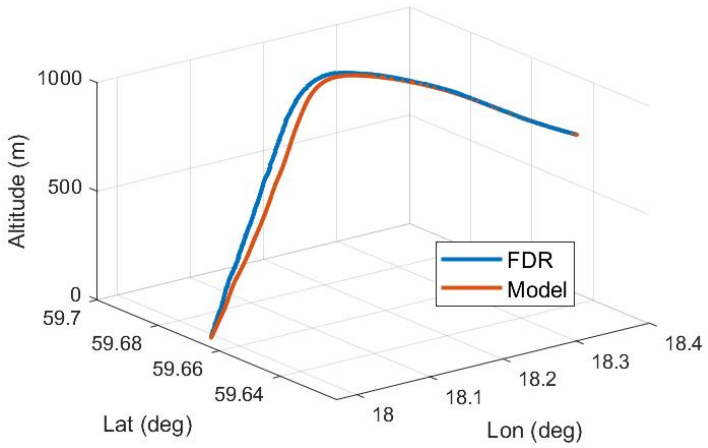

Figure 2.5: 3D flight path comparison.

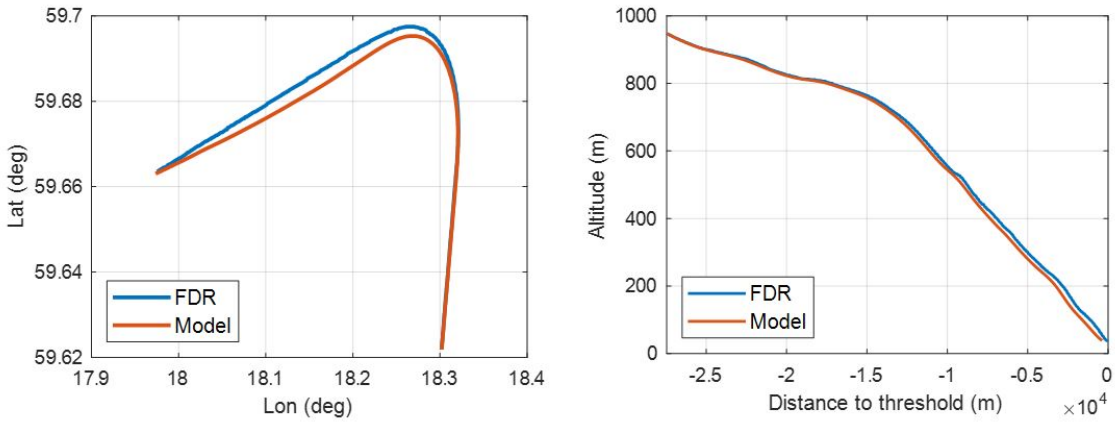

Figure 2.6: Horizontal and vertical flight path comparison.

Even though the full set of the state equations, eq. 2.14, could not be integrated, accounting for all of the above results and comments, it is believed that the model is sufficiently accurate to simulate realistic trajectories and be used in further studies.

Chapter 3

Noise Modelling Methods

This section is dedicated to the description of the methods included in the noise models. More specifically, a brief description of the noise source models together with a validation example are provided. The propagation and atmosphere models implemented in CHOICE are also described. Typically, the required inputs for the noise source models, implemented in CHOICE, are generated by GESTPAN and WEICO. GESTPAN generates performance data and WEICO provides conceptual design data for the engine. The noise models implemented in CHOICE need input from both models.

3.1 Sound source models

The noise estimation is based on empirical and semi-empirical noise source models found in public literature. Each component is modelled separately, and the total aircraft noise is calculated as the sum of all the individual components. This section is dedicated to the introduction of all implemented models for every component.

3.1.1 Fan and compressor noise

The model used for the prediction of noise from the fan and the compressor components is based on the method introduced by Heidmann [30] and later updated by Kontos et al. [39]. The predicted noise is in 1/3 octave band frequencies of the free field noise pattern, which for the fan and the compressor inlet consists of broadband, discrete tone and combination tone noise and for the fan discharge consists of broadband and discrete tone noise. The parameters required to predict basic noise spectrum levels are the mass flow rate, the total temperature rise for a fan or compressor stage and the design and operating point values of the rotor tip relative inlet Mach number.

Broadband noise is generally attributed to random unsteadiness or turbulence in the flow passing the blade. This unsteadiness can be caused by turbulence in the wall and blade boundary layers, in the blade wakes and vortices, or in the freestream inlet flow. Another possible cause of broadband noise is the modulation of a tone generating mechanism.

Discrete tones are observed at integer multiples of the fundamental blade passage frequency. They appear in either subsonic or supersonic tip speeds and are caused by lift fluctuations on rotor or stator blades. The main sources of lift fluctuations are the inlet flow turbulence or distortion, inlet guide vanes trailing wakes and rotor blades trailing wakes. The peak characteristic sound pressure level for all noise components, except the combination tone noise, is described by the following equation

$$L_c = 20\log\left(\frac{\Delta T}{\Delta T_0}\right) + 10\log\left(\frac{\dot{m}}{\dot{m}_0}\right) + F_1(M_{trd}, M_{tr}) + F_2(RSS) + F_3(\theta) \tag{3.1}$$

where $\Delta T/\Delta T_0$ is the temperature rise across the fan or compressor stage, normalized by a reference value, $\dot{m}/\dot{m}_0$ is the mass flow rate through the component over a reference mass flow rate, M_{trd} and M_{tr} are the rotor tip relative inlet Mach number at design and operating point, RSS is the rotor-stator spacing and θ is the angle between the observer and the engine inlet or directivity angle. The values for F_1, F_2 and F_3 are taken from graphs provided in [30] and [39] and vary for every component.

Then, the sound pressure level spectrum for inlet broadband and discharge broadband and discrete tone noise is obtained from

$$SPL(f) = L_c + F_4(f/f_b) \tag{3.2}$$

while for inlet discrete tone noise from

$$SPL(f) = L_c + 10\log\left(10^{0.1F_4\left(\frac{f}{f_b}\right)} + 10^{0.1F_5\left(\frac{f}{f_b}\right)}\right) \tag{3.3}$$

where F_4 and F_5 are represented by functions provided in the reports and they differ for each component.

For the combination tone noise, the characteristic peak level at center frequencies one-half, one-fourth and one-eighth of the fundamental blade passage frequency is given by

$$L_c = 20\log\left(\frac{\Delta T}{\Delta T_0}\right) + 10\log\left(\frac{\dot{m}}{\dot{m}_0}\right) + F_1(M_{tr}) + F_2(\theta) + C \tag{3.4}$$

where F_1 and F_2 are provided in figures and C equals -5 dB for a fan with inlet guide vanes and 0 for a fan without inlet guide vanes. The sound pressure level spectrum for each of the three combination tone components is obtained from

$$SPL(f) = L_c + F_3(f/f_b) \tag{3.5}$$

where F_3 is provided in the relevant figure in the report.

The total combination tone noise sound pressure level spectrum is obtained by summing the spectrum of each of the three components on an energy basis.

3.1.2 Core noise

The combustor noise source model is based on the model described by Gliebe et al. [21] for low-emissions combustors. Farfield noise data were collected and analyzed for both SAC (Single-Annular Combustor) and DAC (Dual-Annular Combustor) and two correlations were developed taking into account the combustor geometry, cycle conditions, spectral frequency content and directivity.

Single-annular combustor

The spectral noise peaks for single-annular combustors are observed in three frequencies and directivities: 63, 160 and 630 Hz and 150^o, 130^o and 130^o, respectively. The procedure to calculate the overall sound pressure level starts from computing the normalized OASPL (Overall Sound Pressure Level) for every spectral peak.

$$OASPLN = \begin{cases} -67.8\theta_n^2 + 141.7\theta_n - 66.84, & f_p = 63Hz \\ -26.019\theta_n^3 - 5.2974\theta_n^2 + 93.43\theta_n - 67.75, & f_p = 160Hz \\ -156.5\theta_n^2 + 322.34\theta_n - 164.89, & f_p = 630Hz \end{cases} \tag{3.6}$$

where θ_n is the normalized given directivity angle with the peak angle defined as $\theta_n = \theta/\theta_p$.

The OASPL is, then, computed for every peak frequency as

$$OASPL(\theta) = \begin{cases} OASPLN + OASPL(\theta_p) + 0.40\left(SPL(F_C) - SPL(T_L)\right), \\ f_p = 63Hz \\ OASPLN + OASPL(\theta_p) + 0.10\left(SPL(F_C) - SPL(T_L)\right), \\ f_p = 160Hz \\ OASPLN + OASPL(\theta_p) + 0.30\left(SPL(F_C) - SPL(T_L)\right), \\ f_p = 630Hz \end{cases} \tag{3.7}$$

where $SPL(F_C)$ and $SPL(T_L)$ are the combustor flow and turbine nozzle transmission-loss related effects, given by

$$SPL(F_C) = 20\log(F_C) \tag{3.8}$$

$$SPL(T_L) = 20\log(T_L) \tag{3.9}$$

and

$$F_C = \frac{W_3\sqrt{T_4 - T_3}}{P_3 A_{EC}^2\sqrt{N_f}} \tag{3.10}$$

$$T_L = \frac{(1 + F_T)^2}{(4L_C F_T)/(\pi h)} \tag{3.11}$$

$$F_T = \left(\frac{P_4}{P_7}\right)\left(\frac{T_7}{T_4}\right)^{(1/2)} \tag{3.12}$$

where W_3 is the combustor inlet flow in lbm/s, T_4 the combustor exit temperature in ^oR, T_3 the combustor inlet temperature in ^oR, P_3 the combustor inlet pressure in $psia$, A_{EC} the combustor exit area in ft^2, N_f the number of ignited fuel nozzles, L_C the combustor nominal length in ft, h the annulus height at combustor exit in ft, P_4 the combustor exit pressure in $psia$, P_7 the pressure of the turbine last stage in $psia$ and T_7 the temperature of the turbine last stage in ^oR. The pressure

and temperature refer to their total values. The peak overall sound pressure level is computed as

$$OASPL(\theta_p) = \begin{cases} -20\log(R) + H_{CP}\left(30/N_f\right)^{-0.225}, & f_p = 63Hz \\ -20\log(R) + H_{CP}\left(30/N_f\right)^{0.050}, & f_p = 160Hz \\ -20\log(R) + H_{CP}\left(30/N_f\right)^{0.020}, & f_p = 630Hz \end{cases} \tag{3.13}$$

$$H_{CP} = \begin{cases} 76.45 + 14.256\log(CP), & f_p = 63Hz \\ 108.5 + 3.31\log(CP), & f_p = 160Hz \\ 106.38 + 6.938\log(CP), & f_p = 630Hz \end{cases} \tag{3.14}$$

$$CP = \frac{W_3\sqrt{T_3}}{P_3}\frac{T_4 - T_3}{T_4}\frac{P_3}{P_0}\left(\frac{D_h}{D_e}\right)^{0.50} \tag{3.15}$$

where R is the observation radius which is assumed equal to $150ft$, P_0 is the reference ambient pressure in $psia$, D_h and D_e are the exhaust nozzle exit plane effective and hydraulic diameters in ft.

The normalized sound pressure level as a function of normalized frequency is calculated as

$$SPLN(f_n) = \begin{cases} -152.70 + 295.46f_n - 145.61f_n^2, & f_p = 63Hz \\ -170.07 + 331.33f_n - 163.34f_n^2, & f_p = 160Hz \\ -147.50 + 286.40f_n - 142.31f_n^2, & f_p = 630Hz \end{cases} \tag{3.16}$$

Finally, the spectrum is determined for every frequency and directivity as

$$SPL(\theta, f) = OASPL(\theta) + SPLN(f_n) + AA\frac{R_0}{1000} \tag{3.17}$$

where AA is the air attenuation factor in dB per $1000ft$.

Dual-annular combustor

Dual-annular combustors were found to peak at two frequencies, 160 and 500 Hz, with one peak observer angle at 130^o. The normalized overall sound pressure level is, in this case, computed as

$$OASPLN = \begin{cases} -116.95\theta_n^2 + 235.23\theta_n - 120.65, & f_p = 160Hz \\ -137.59\theta_n^2 + 283.40\theta_n - 147.73, & f_p = 500Hz \end{cases} \tag{3.18}$$

The overall sound pressure level is given by

$$OASPL(\theta) = \begin{cases} OASPLN + OASPL(\theta_p) + 0.45\left(SPL(F_C) - SPL(T_L)\right), \\ f_p = 160Hz \\ OASPLN + OASPL(\theta_p) - 0.10\left(SPL(F_C) - SPL(T_L)\right), \\ f_p = 500Hz \end{cases} \tag{3.19}$$

where $SPL(F_C)$ and $SPL(T_L)$ are the combustor flow and turbine-related corrections, given by eq. 3.8 and eq. 3.9, but with

$$F_C = \frac{W_3\sqrt{T_4 - T_3}}{P_3 A_{EC}^2 \sqrt{20 + N_f}} \tag{3.20}$$

where N_f is now the number of inner-row fuel nozzles ignited.

The overall sound pressure level for every peak angle is a function of the fuel-nozzles staging and is defined as

$$OASPL(\theta_p) = K_{NF}\left(-20\log(R) + H_{CP}\left(\frac{20+N_f}{N_{f,max}}\right)^{-X_K}\left(\frac{30}{20+N_f}\right)^{M_f}\right) \tag{3.21}$$

where $M_f = 0.020$ for $f_p = 160Hz$ and $M_f = 0.180$ for $f_p = 500Hz$. The parameters K_{NF} and X_K vary with spectral peak frequency and fuel nozzle firing pattern and can be obtained from the relevant table in [21]. The coefficient H_{CP} is given by

$$H_{CP} = \begin{cases} 76.45 + 14.256\log(CP), & f_p = 160Hz \\ 110.62 + 2.997\log(CP), & f_p = 500Hz \end{cases} \tag{3.22}$$

$$CP = \begin{cases} \frac{W_3\sqrt{T_3}}{P_3}\frac{T_4-T_3}{T_4}\frac{P_3}{P_0}\left(\frac{D_h}{D_e}\right)^2, & f_p = 160Hz \\ \frac{W_3\sqrt{T_3}}{P_3}\frac{T_4-T_3}{T_4}\frac{P_3}{P_0}\left(\frac{D_h}{D_e}\right)^{1.20}, & f_p = 500Hz \end{cases} \tag{3.23}$$

Finally, the spectra are calculated from eq. 3.17 with the normalized sound pressure level computed as

$$SPLN(f_n) = \begin{cases} -170.07 + 331.33 f_n - 163.34 f_n^2, & f_p = 160Hz \\ -137.21 + 268.99 f_n - 135.81 f_n^2, & f_p = 500Hz \end{cases} \tag{3.24}$$

3.1.3 Turbine noise

The method implemented for turbine noise is described by Dunn and Peart [13] and consists of broadband and discrete tone noise components which are related to the last stage relative tip velocity, the primary mass flow and local speed of sound at the turbine exit. The discrete tone noise is also dependent on the stator/rotor spacing. The spectra for both components are normalized with respect to the fundamental blade passage frequency of the last stage of the turbine and are given in 1/3 octave band levels ($dB\ re\ 20\ \mu Pa$) at the free-field, index ($R = 1m$) conditions.

The broadband noise component for the peak 1/3 octave band level at a radius of 45.7 m from the source is given by

$$L_0 \cong 10\log\left(\left(\frac{V_{TR}C_0}{V_0 C_L}\right)^3 \frac{\dot{m}}{\dot{m}_0}\left(1 - M\cos(\xi)\right)^{-4}\right) + F_1(\theta) - 10 \tag{3.25}$$

where V_{TR} is the relative tip speed of last rotor of the turbine (0.7 times the tip speed is used if V_{TR} is unknown), V_0 is the reference velocity equal to 0.305 m/s,

$\dot{m}$ is the primary mass flow, $\dot{m}_0$ is the reference mass flow equal to 0.4536 kg/s, C_L is the speed of sound at the turbine exit ($C_L = a\sqrt{T_{T7}}$) with $a = 19.8m/s$ per $(^oK)^{0.5}$, if it is unknown), C_0 is the reference speed of sound equal to 340.3 m/s, M is the aircraft Mach number, ξ is the angle between direction of aircraft and sound propagation path, θ is the directivity angle relative to the inlet axis and F_1 is given by the empirical curve in Figure 52 of reference [13].

The sound pressure level spectrum at 45.7 m from the source can be obtained from

$$SPL(f) \mid_{45.7m} \cong L_0 + F_2(f/f_0) \tag{3.26}$$

where $f_0 = B\dot{\theta}/\left(60\left(1 - M\cos\left(\xi\right)\right)\right)$ is the fundamental blade passage frequency of the last stage of the turbine, B is the number of blades for the last rotor stage of the turbine, $\dot{\theta}$ is the shaft speed in rpm and F_2 is provided in Figure 54 of reference [13].

Similarly, the discrete tone component at a radius of 45.7 m from the source is calculated by

$$L_0 \cong 10\log\left(\left(\frac{V_{TR}}{V_0}\right)^{0.6}\left(\frac{C_0}{C_L}\right)^3 \frac{\dot{m}}{\dot{m}_0}\left(\frac{c}{s}\right)\left(1 - M\cos\left(\xi\right)\right)^{-4}\right) + F_1(\theta) + 56 + K \tag{3.27}$$

where c/s is the stator/rotor spacing and K is a correction factor for turbofans with a primary nozzle exit plane upstream of the secondary nozzle exit plane, i.e. the JT8D. K is equal to -10 dB for the JT8D and 0 dB for dual exhaust systems with co-planar exits or turbojets.

The tones are added to the broadband spectrum, computed by eq. 3.26, and a correction is applied for the use of multiple engines and free-field conditions, as follows

$$SPL(f) \mid_{1m} = SPL(f) \mid_{45.7m} + 33.2 + \Delta dB(f) \tag{3.28}$$

where $\Delta dB(f)$ is obtained from Table 4 in reference [13].

3.1.4 Jet noise

Jet noise is modeled as presented by Russel [48]. This method can be used to estimate source noise both from circular and coaxial jets, and it is based on extensive test data. The sound pressure levels from the test data are curve fitted, as a function of frequency and directivity, using bicubic splines and a third order Taylor series. The component noise levels are then defined for all frequencies and directivities.

The coaxial jet noise is calculated as a function of the jet state properties for a single stream equivalent jet with the same mass flow, energy flow and thrust as the coaxial jet. These properties are the normalized equivalent jet velocity, the normalized equivalent jet total temperature, the velocity ratio of the outer stream to the inner stream, the temperature ratio and the area ratio. The 1/3 octave band sound pressure level is calculated as the summation of four components

$$SPL(\theta, \eta) = \overline{OAPWL} + D(\theta) + F(\eta) + RSL(\theta, \eta) + k_1 + k_2 + k_3 \tag{3.29}$$

where $\overline{OAPWL}$ is the normalized overall power level, $D(\theta)$ the directivity index, $F(\eta)$ the power spectrum level and $RSL(\theta, \eta)$ the relative spectrum level. The parameters

k_1, k_2 and k_3 are constants that depend on the size of the jet, the microphone distance, the ambient conditions and the ratio between the reference power level and the reference mean square pressure level. The frequency parameter, η, is used instead of the frequency and is defined as

$$\eta = 10 \log \left(\frac{f D_e}{V_e} \right) \tag{3.30}$$

where D_e is the equivalent diameter of the coaxial or circular jet and V_e the nozzle exit equivalent flow velocity.

The four components in eq. 3.29 are empirically defined as a function of flow state parameters on each point of a grid, which consists of seven directivity coordinate points, $\theta_c = 0^o, 30^o, 60^o, 90^o, 120^o, 150^o, 180^o$ and seven frequency parameter coordinate points, $\eta_c = -1.5, -1.0, -0.5, 0.0, 0.5, 1.0, 1.5$. More specifically, they are computed by multiplying and summing their corresponding derivative values, obtained from the relevant tables in reference [48], with the derivative multiplier values, X_j. The derivative multipliers vary from 8 for the circular jet to 36 for the coaxial jet. They are obtained from a least square fit Taylor series and can be defined according to Table III in the same report, accounting for the exit flow parameters, which are computed using the equivalent jet flow properties as follows

$$x_i = \log \left(\frac{a_i}{a_{ir}} \right) \tag{3.31}$$

where a_i is the i_{th} prediction parameter or equivalent jet state property and a_{ir} is the standard value for the i_{th} prediction parameter.

Finally, with the four components determined at the reference coordinate points, cubic splines are used to obtain them in all directivities and frequencies and the sound pressure level is calculated.

3.1.5 Airframe noise

For the airframe noise prediction a combination of methods found in the public literature is implemented. This can be supported by the assumption that the dominant airframe noise sources are the trailing-edge diffracted quadrupole sound, generated principally at the wing and flap trailing edges and the point dipole sources, caused by the landing gear.

Trailing-edge noise

The trailing-edge noise is modelled according to the method proposed by Hersh et al. [31] which is based on the trailing-edge diffraction theory of Ffowcs Williams and Hall. In this theory, they concluded that the sound caused by a diffracting edge is proportional to the fifth power of the free-stream velocity. The maximum overall sound pressure level is then computed from

$$OASPL_w = 10 \log \left(\frac{K_w C_{Dw} \rho^2 V^{4.8} S_w \cos^2(\theta/2) \sin(\phi) \cos^2(\psi)}{p_0 a R^2 (\bar{c}/\nu)^{0.2}} \right) \tag{3.32}$$

where V is the aircraft speed in m/s, S_w the aircraft reference area in m^2, θ and ϕ the longitudinal and lateral directivity, respectively, ψ the wing sweep angle, p_0 the reference sound pressure equal to 20 μPa, a the local speed of sound, R is the distance between the observer and the source (1 m for free-field conditions), $\bar{c}$ the wing aerodynamic chord in m and ν the kinematic viscocity in m^2/sec. K_w is a constant that represents the average of the variation of the edge-scattering noise along the aircraft wing. If other configuration than clean is used, this constant is substituted with K_{wf}. The values for these constants can be found in the report by Lasagna et al. [42]. Finally, C_{Dw} is the wing drag coefficient which is estimated as suggested by Raymer [47], as the sum of the wing zero-lift drag (for clean configuration), the drag due to lift and any drag increase caused by the flap deflection.

The 1/3 octave band sound pressure level is then calculated using the following equation which is taken from the airframe sub-component model developed by Golub et al. [23]

$$SPL(f) = a_6X^6 + a_5X^5 + a_4X^4 + a_3X^3 + a_2X^2 + a_1X + a_0X + OASPL_w \quad (3.33)$$

$$X = \log\left(f\xi_l t_f/V\right) \quad (3.34)$$

where ξ_l is the length scale factor, t_f the outboard flap edge chord and the constants a_0 through a_6 can be found in [23].

Landing gear noise

The landing gear noise is modelled empirically as proposed by Guo [29]. According to this method, the noise from the landing gear can be decomposed into three main spectral components, low-, mid- and high- frequency. The first one is generated by the wheels, the second by the main struts and the third by small details. The total noise is the summation of the three components and can be expressed as

$$\langle p^2\rangle = \frac{(\rho_0 c_0^2)^2 M^6 e^{-aR} D_0(\theta)}{R^2(1 - M\cos\theta)^4}\{P_L + P_M + P_H\} \quad (3.35)$$

where e^{-aR} refers to the atmospheric absorption, $D_0(\theta)$ is a directivity factor to account for the installation effects and each component is represented by the parameter P which is defined by

$$P = \beta S_l D(\theta) F(St) \quad (3.36)$$

with β the radiation efficiency, S_l the aggregated surface of the landing gear parts in each group, $D(\theta)$ the directivity factor for isolated landing gears and $F(St)$ the normalized spectrum. The values and equations for these parameters for each of the three frequency components can be found in [29].

The sound pressure level can then be computed from

$$SPL(f) = 20\log\left(\frac{p}{p_0}\right) \quad (3.37)$$

3.1.6 Noise suppression

The source prediction methods for the fan and the turbine described in the previous sections result in a slight overprediction of the noise level. This can be attributed to several factors with the most dominant one being that both methods refer to hardwall prediction and no acoustic treatment is included. The effect of acoustic treatment becomes even more prominent as technology advances and since these methods were developed based on older engine models it is necessary to account for any noise reduction mechanisms. An example of the noise reduction in the fan and turbine components due to acoustic treatment is presented in Figure 3.1. In the same figure, the contribution of the individual components on the total noise level for the approach and take-off segments is also indicated. The original figure can be found in the report by Groeneweg and Rice [26], where a detailed discussion regarding fan noise generation and suppression and the mechanisms involved is provided. Further discussion on aircraft noise reduction technologies can be found in several review articles, such as the bibliographic review presented by Casalino et al. [6] and in the overview presented by Leylekian et al. [43].

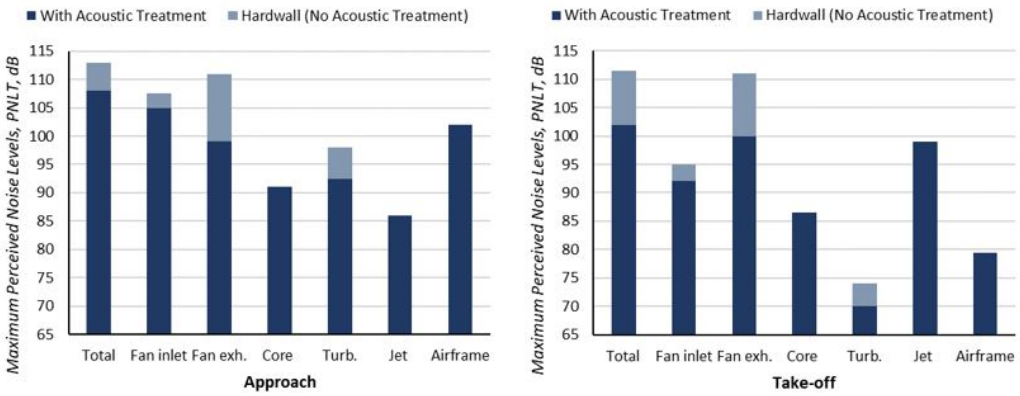

Figure 3.1: Effect of acoustic treatment on engine components. Figure reproduced from [26].

Regarding the fan noise, another possible reason for the overprediction is that that the model was developed based on measurements from static fan tests. During such tests, ingestion of vortices or other turbulence from the test stand or other nearby structures can interfere with the data, as described by Krejsa and Stone [40].

Krejsa and Valerino [41] compared several semi-empirical turbine noise prediction methods with measurements and concluded that the most accurate prediction was provided by the Dunn and Peart method [13], that was introduced in Section 3.1.3. However, they found that even this method resulted in a significant deviation ranging from -6 to 8 dB. They suggested that the method should be reevaluated and modified as more data become available. Following this comment, no further updates or more recent correlations have been found.

Considering the above, a simple noise suppression module has been implemented, where a suppression factor is set and applied for every frequency and directivity. The method was described by Wilson [59] and can be applied to any component

but is mainly used for the fan inlet, fan discharge and turbine components. The implementation of the factor is described by the following equations.

$$\langle p^2 \rangle_S = \langle p^2 \rangle S \tag{3.38}$$

$$S = 10^{S_{dB}/10} \tag{3.39}$$

where S_{dB} is the desired suppression (negative value) in dB, S the suppression factor and $\langle p^2 \rangle$ and $\langle p^2 \rangle_S$ the unsuppressed and suppressed mean square acoustic pressure, respectively. Indicative values for the suppression can be found in the report by Willshire and Garber [58].

3.2 Propagation effects

The noise received by the microphone or an observer on the ground is subject to several propagation and attenuation effects. These include lateral attenuation, ground reflection, Doppler-shift effect, spherical spreading and atmospheric absorption. These effects are briefly presented in this section.

3.2.1 Lateral attenuation

Lateral attenuation refers to the difference between the sound level in a location under the aircraft and the level in a location at the side of the aircraft. This difference usually occurs due to engine-installation effects, ground surface absorption and refraction and scattering due to wind and other meteorological effects. The sound level at the side of the aircraft is usually less than under it and can, therefore, be modelled as [49]

$$L_{lateral} = L_{under} + \Lambda \tag{3.40}$$

where $L_{lateral}$ and L_{under} is the sound level at the side and under the aircraft, respectively, and Λ is the total lateral attenuation which is computed from the following equation

$$\Lambda(\beta, l, \phi) = E_{Eng}(\phi) - \frac{G(l) A_{Grd+RS}(\beta)}{10.86} \tag{3.41}$$

with E_{Eng} the engine installation effect, ϕ the depression angle (^{o}), $G(l)$ the over-ground attenuation, l the lateral distance, A_{Grd+RS} the ground and refraction-scattering effects and β the elevation angle (^{o}). These effects are modelled according to the following equations.

$$E_{Eng}(\phi) = \begin{cases} 10 \log \left(0.1225 \cos^2(\phi) + \sin^2(\phi)\right)^{0.329}, & \text{fuselage-mounted engine} \\ 10 \log \left(\frac{(0.0039 \cos^2(\phi) + \sin^2(\phi))^{0.062}}{0.8786 \sin^2(2\phi) + \cos^2(2\phi)} \right), & \text{wing-mounted engine} \\ 0, & \text{propeller-driven aircraft} \end{cases} \tag{3.42}$$

$$G(l) = 11.83 \left(1 - e^{-2.74 \times 10^{-3} l}\right) \tag{3.43}$$

$$A_{Grd+RS}(\beta) = \begin{cases} 1.137 - 0.0229\beta + 9.72 e^{-0.142\beta}, & 0^o \leq \beta \leq 50^o \\ 0, & 50^o < \beta \leq 90^o \end{cases} \tag{3.44}$$

3.2.2 Ground reflection

Ground reflection occurs when the sound waves from a source to an observer are not travelling directly but instead they are reflected on the ground and can either increase or reduce the sound intensity. Modelling of this effect is based on the method presented by Zorumski [64]. This method is based on the Chien-Soroka theory which assumes that the ground is a locally reacting uniform plane and that the aircraft is a point source. The mean square acoustic pressure, with the ground effect included, is calculated by

$$\langle p^2 \rangle_{gr} = \langle p^2 \rangle_{ff} \left(1 + R^2 + 2RC \cos\left(a + k\Delta r\right) \frac{\sin((K-1)k\Delta r)}{(K-1)k\Delta r} \right) = \langle p^2 \rangle_{ff} G \quad (3.45)$$

where $\langle p^2 \rangle_{ff}$ is the free-field mean square acoustic pressure, R and α are the magnitude and argument of complex spherical-wave reflection coefficient, respectively, and $K = 2^{1/(6N_b)}$, with N_b the number of sub-bands per 1/3 octave band. The term in the parenthesis is symbolised with G and represents the ground-effects factor. C is the coherence coefficient computed from the following equation

$$C = e^{-(ak\Delta r)^2} \quad (3.46)$$

with k the wave number and Δr the path-length difference, as presented in Figure 2 in [64], equal to

$$\Delta r = 2h \cos\left(\theta\right) \quad (3.47)$$

3.2.3 Doppler effect

This effect is well known and states that the frequency of a wave reaching an observer standing still will be shifted compared to the emitted frequency from a moving source. This has direct application in any moving vehicle and should, therefore, be accounted for in aircraft pass-by noise. The frequency received by the observer is calculated by

$$f_{observer} = \frac{f_{source}}{1 - M \cos\left(\theta\right)} \quad (3.48)$$

where θ is the angle between the flight velocity and the direction of sound propagation to the observer.

3.2.4 Spherical spreading

Spherical spreading describes the phenomenon of uniform wave propagation away from a point source in all directions. If the emitted acoustic power from the source is equal in all directions, its distribution must remain constant over any sphere around the source. Therefore, the power transmitted per unit area, i.e. the acoustic intensity, decreases proportionally with $1/R^2$, where R is the radius of the sphere and the area of the sphere increases with R^2. Hence, the noise received by an observer on the ground is highly dependent on the distance between the aircraft and the observer.

3.2.5 Atmospheric absorption

An emitted sound wave from an aircraft travels through the atmosphere causing its magnitude to decrease due to two main mechanisms. The first mechanism is the classical absorption which is a result of energy dissipation due to viscous losses and heat conduction and depends on the temperature and the frequency. The second mechanism is the molecular absorption which is a function of frequency, temperature and humidity and is caused by rotational and vibrational relaxation processes of oxygen and nitrogen. These two terms are modelled according to the SAE ARP 866A report [50] as

$$\alpha(f) = \alpha_{classical} + \alpha_{mol} \tag{3.49}$$

$$\alpha_{classical} = 10^{\left(2.05 \log\left(\frac{f}{1000}\right) + 1.1394 \times 10^{-3} T - 1.916984\right)} \tag{3.50}$$

$$\alpha_{mol} = \alpha_{molmax} \times \alpha_{normalized} \tag{3.51}$$

$$\alpha_{molmax} = 10^{\left(\log(f) + 8.42994 \times 10^{-3} T - 2.755624\right)} \tag{3.52}$$

3.3 Noise source model validation

An extensive validation study regarding the source noise prediction has been performed based on FDR and noise measurement data. In the present thesis, only a brief description of the validation process and some example results will be presented, as this concerns on-going work that is planned to be published soon, together with an open-access version of the noise prediction code (CHOICE).

3.3.1 Data availability and processing

The available data were collected as part of the ANT (Approach Noise Trials) project [1] at the CSA. The flights were performed by two Novair A321neo with Leap-1A engines and all the measurements were taken during the morning of April 8th, 2021. The flights were conducted purely for noise measurement purposes and each aircraft performed 10 approach flyovers. Around 25 microphones were placed along a 15 nm approach path and at a height of 1.2 m above ground. This was done on runway 26 at Arlanda. A detailed description of the measurements set up is presented by Åbom et al. [1].

The ground noise data were A-weighted and given in 1/3 octave band frequencies in 1 sec resolution. The post processing was performed by Tengzelius and Johansson [54] and through a back-propagation process the source level was estimated. The FDR data were in the same format as the set that was used for the 4D trajectory model development and verification and the model described in Chapter 2 was used to calculate all the required parameters for the noise prediction.

3.3.2 Noise source prediction

The first step for the noise source prediction is the trajectory performance. Since FDR data were available, the trajectory model was applied to estimate any missing parameters required for the noise prediction, such as the thrust and wing drag coefficient. The engine performance was simulated using the in-house code GESTPAN, which has been setup to require thrust, airspeed, altitude and ambient conditions to generate several performance files for each of the engine's components. The engine mechanical design data are, then, generated by WEICO. CHOICE takes the engine and aircraft performance and dimensions files and a trajectory file and the noise is calculated for every point along the trajectory. The output from CHOICE is a frequency and directivity dependent SPL matrix for every trajectory point.

3.3.3 Sample results

In order to compare the prediction with the back-propagated measurements, the results were divided according to the aircraft configurations presented in Table 2.1. For every configuration the SIL (Sound Intensity Level) spectra at the source and directly underneath the aircraft (longitudinal and lateral directivity equal to 90^o) are compared. As an example, the comparison for configuration FULL is presented in Figure 3.2. The mean spectra for every microphone and the overall mean is presented, considering only the microphones that were directly overflown, i.e. measurements with lateral directivity smaller than 80^o were disregarded. The average speed that the aircraft had when over-passing each microphone is also visible in the figure.

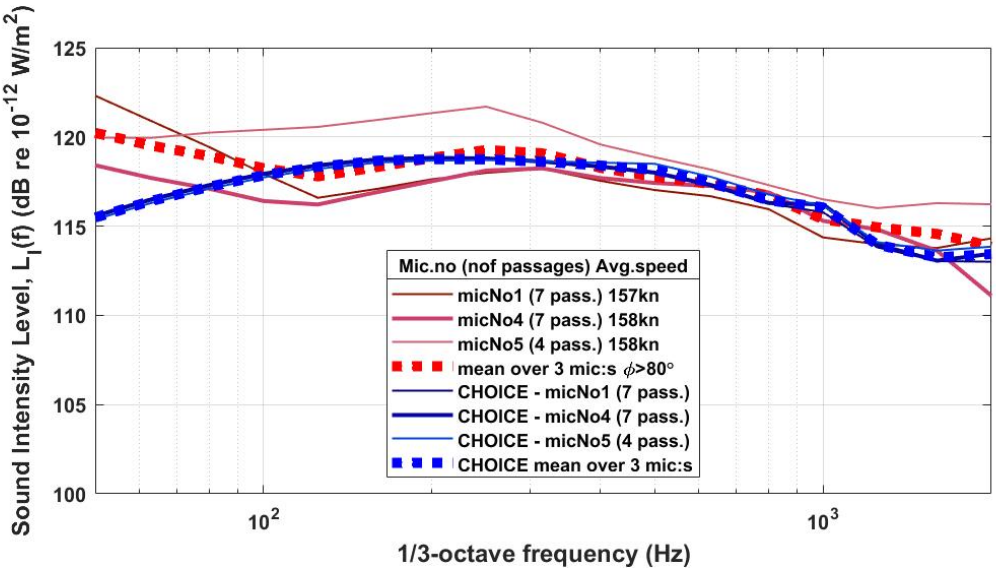

Figure 3.2: Measured and estimated SIL, at the source, for configuration FULL.

For the presented sample case in Figure 3.2, both the level and the shape of the spectra match well. The estimated mean spectrum for each microphone does not show any significant variation as the aircraft speed and engine operating conditions were similar. The shapes of the two spectra are slightly different in the low-frequency

region. The back-propagated source level indicates a gradual increase for frequencies below 100 Hz. One possible explanation is that a stronger flow separation occurs due to the higher flap angle. On the contrary, geometric characteristics are not considered in detail in the implemented airframe model, for trailing-edge source noise, and effects like this cannot be well represented. Despite the aforementioned deviations, it is believed that the source noise level for configuration FULL is well predicted from the model.

Chapter 4

Summary of Papers

4.1 Paper 1

In Paper 1, a system-level study was performed in order to assess the environmental impact of early design choices for an ultra-high bypass ratio turbofan engine. The aim was to quantify the effect of engine cycle parameter variation on noise and NO_x emissions within a range close to the optimal engine condition where only a small penalty in fuel burn would be incurred.

4.1.1 Methodology description

For this study, a model was set up for a state-of-the-art single aisle thrust class turbofan engine. Component efficiencies, cooling technology, component weight and architecture were based on the Leap-1A engine. The aircraft system was modelled to match A321-200.

A Python-based framework combining several in-house codes was used. The engine performance and design were evaluated using GESTPAN and WEICO. GESTPAN was also used to simulate the aircraft performance and establish trajectories by integrating the two dimensional flight dynamics equations. The computed trajectories concerned the LTO cycle and followed the noise certification procedure guidelines. The engine cycle was optimized for minimum installed SFC (Specific Fuel Consumption), by allowing variation in OPR, FPR and BPR, while keeping the aircraft characteristics and the trajectories fixed. For the optimization, OpenMDAO was used, which is an open-source framework for multidisciplinary optimization, introduced by Gray et al. [24]. Around the optimum point, two case studies were defined, one for varying OPR and one for varying FPR and BPR. Trades were, then, evaluated between noise at the certification points and LTO emissions. Noise predictions were carried out using CHOICE and the methods presented in Chapter 3. NO_x emissions were computed using CHEESE (CHalmers Engine Emissions Simulation Environment) which is based on semi-empirical modeling methods [25].

4.1.2 Discussion

For the optimization, an installed SFC metric was selected as the objective function. This was expected to be a better metric than pure SFC as it accounts for the effect of the nacelle drag and engine weight. For both scenario studies, it was observed that with only a modest increase in the installed SFC metric, a large variation in cycle parameters could be achieved. This variation in engine parameters proved to be significant regarding the noise and emissions. Even though the OPR variation did not have a notable effect on noise, the decrease in total NO_x mass was significant, amounting to 12% reduction from the optimum installed SFC case. On the other hand, varying the fan diameter within a range not leading to a substantial increase in installed SFC resulted in a considerable improvement in engine noise equal to 1.7 dB, and additionally giving a slight benefit in estimated NO_x emissions.

4.2 Paper 2

In Paper 2, interdependencies between noise and emissions were evaluated for aircraft operational procedures. Focusing on approach procedures, the aim was to assess the environmental impact of standard, more advanced and optimized noise abatement trajectories.

4.2.1 Methodology description

The trajectories were constructed based on available FDR data and theory found in operating manuals and similar studies. The ground path was kept constant for all study cases and only the vertical profile was varied according to the studied procedure. The aircraft performance was evaluated using the models developed in Chapter 2, followed by GESTPAN simulations to evaluate the engine performance and by CHOICE and CHEESE simulations for the prediction of noise and NO_x emissions. For this study, the noise mapping tool SAFT [51] was used in connection with CHOICE in order to generate SEL contours under the aircraft flight path.

An optimization study was performed using a multiobjective Genetic Algorithm. The objective was to minimize the noise impact for a community located underneath the flight path and the total mission NO_x emissions. The process started from a conventional approach trajectory and the objectives were normalized according to this procedure.

All cases were presented for an aircraft/engine model based on the A321neo with Leap-1A engine at Arlanda airport in Stockholm.

4.2.2 Discussion

Several approach procedures were evaluated for their environmental impact. The analysis started from noise abatement procedures, namely the CDA and LDLP, and other standard trajectories, such as the conventional and the multi-level approach. Based on these, more advanced trajectories were explored such as a CDA with a

steeper descent angle, a segmented CDA and an LDLP with a shorter intermediate level segment. It was shown that there is no single better trajectory but the selection of the appropriate procedure is highly dependent on the airport, flight conditions, atmospheric conditions and aircraft type. From the results it was observed that, in general, if a procedure leads to noise reduction in proximity to the airport this is traded with increased noise level further away. The more advanced procedures seemed to result in increased NO_x emissions while the effect on the fuel consumption was not that evident. This can be explained by the fact that contrary to CO_2 and SO_x emissions, NO_x emissions also depend on the climate and local weather conditions.

As expected, the optimization resulted in the best solution from the studied trajectories and for the selected scenario. Even though noise was minimized for a specific location, an overall improvement was observed. NO_x emissions were significantly improved but a slight increase in the fuel consumption was observed, as it was not accounted for in the optimization. The increase in CO_2 and SO_x emissions was rather small and was considered acceptable for the achieved noise and NO_x emissions reduction.

Chapter 5

Concluding Remarks

5.1 Summary

A physics based method for computing 4D single flight trajectories has been developed and verified using FDR data. It was demonstrated that the model can accurately predict aerodynamic parameters and aircraft position and simulate realistic flight trajectories. This was a necessary first step for studies regarding the noise and emissions prediction, especially in connection with the evaluation of operational procedures.

The noise prediction methods have been described in detail. Most of the methods were already implemented in CHOICE, but some modifications have been made in connection with the validation study, a brief description of which was presented in Section 3.3.

Using the described tools, two studies were performed, focusing on the evaluation of intedependencies between noise and emissions. The first study was concerned with the engine technology evaluation and how fuel burn can be traded for noise and emissions reductions. It was demonstrated that significant improvement can be achieved for only a modest effect on the fuel burn. The second study focused on the procedural aspect and on the environmental impact of modifications in approach trajectories and procedures. It was concluded that this is an important measure towards noise and emissions reduction around airports, but it requires adaptation for different airports and conditions.

A conclusion that can be derived from both studies is that when looking to reduce noise pollution from aircraft, it is necessary to treat the combined problem of noise and emissions. Even though noise does not directly affect the environment, it was clearly shown that any low noise solution influences both CO_2 and NO_x emissions. It is, therefore, important to consider interdependencies when new designs or procedures are proposed.

5.2 Future work

From this point forward, it is intended that the work on the validation of the noise source models will continue and a detailed analysis of the process is intended for journal publication. The article will be accompanied with a link to an open-access Python version of the physics-based noise prediction code, CHOICE. This is expected to happen in the near future as the Python implementation of the code has already been made and the validation process is completed.

Following this, more scenario studies, where intedependencies are to be evaluated, will be defined and performed. Among the candidate study cases are optimizations of the 4D flight path and evaluation of future aircraft technologies, such as electric aircraft. For the former, all the necessary tools to perform the study are already in place. This study would consist a continuation of the current work. On this basis, a more generalized and user friendly tool could be created, able to generate and optimize 4D approach trajectories for their environmental impact. For the latter, a propeller noise source model would need to be implemented. The study would start from the assessment of the noise impact of electric aircraft and could go into deeper evaluation of future aircraft technology concepts, such as comparing the environmental impact of electric, turboprop and hydrogen aircraft and identifying the most import design parameters in terms of noise generation. The selection of studies will depend on data availability and collaboration with other projects and external partners.

Bibliography

[1] M. Åbom, A. Johansson, K. Bolin, and S. Basu. *Approach Noise Trials*. Technical report for the KTH/Novair project Approach Noise Trials (ANT). Stockholm, Sweden: KTH Royal Institute of Technology, Apr. 2021 (cit. on p. 28).

[2] W. S. Alexander and O. M. Klose. "The Relationship of Wind Correction Angle to Drift Angle". In: *Journal of the Aeronautical Sciences* 8.11 (Nov. 1940), pp. 409–412. DOI: 10.2514/8.10761 (cit. on p. 12).

[3] M. Basner, C. Clark, A. Hansell, J. I. Hileman, S. Janssen, K. Shepherd, and V. Sparrow. "Aviation Noise Impacts: State of the Science". In: 19.87 (Mar. 2017), pp. 41–50. DOI: 10.4103/nah.NAH_104_16 (cit. on p. 3).

[4] L. Bertsch, W. Dobrzynski, and S. Guérin. "Tool Development for Low-Noise Aircraft Design". In: *Journal of Aircraft* 47.2 (Mar. 2010), pp. 694–699. DOI: 10.2514/1.43188 (cit. on p. 7).

[5] E. R. Boeker, E. Dinges, B. He, G. Fleming, C. Roof, P. Gerbi, A. S. Rapoza, and J. Hemann. *Integrated Noise Model (INM) Version 7.0 Technical Manual*. Tech. rep. Washington DC, USA: Office of Environment and Energy, Federal Aviation Administration (FAA), Jan. 2008. URL: https://www.researchgate.net/publication/272026419_Integrated_Noise_Model_INM_Version_70_Technical_Manual (cit. on p. 6).

[6] D. Casalino, F. Diozzi, R. Sannino, and A. Paonessa. "Aircraft noise reduction technologies: A bibliographic review". In: *Aerospace Science and Technology* 12.1 (Jan. 2008), pp. 1–17. DOI: 10.1016/j.ast.2007.10.004 (cit. on p. 25).

[7] *CIDER*. Nov. 2021. URL: https://www.kth.se/csa/projekt/pagaende-projekt/cider-1.979389 (visited on 04/27/2022) (cit. on p. 7).

[8] Civil Aviation Authority (CAA). *Aviation noise and health: The effects of aviation noise*. URL: https://www.caa.co.uk/consumers/environment/noise/aviation-noise-and-health/#:~:text=It%20finds%20that%20above%20dB,to%20hypertensive%20strokes%20and%20dementia. (visited on 04/27/2022) (cit. on p. 3).

[9] Civil Aviation Authority (CAA). *Review of Arrival Noise Controls*. Tech. rep. CAP 1554. Gatwick Airport South, West Sussex: Civil Aviation Authority (CAA), 2017. URL: https://publicapps.caa.co.uk/docs/33/CAP1554ReviewofArrivalNoiseControls_July2017.pdf (cit. on p. 5).

[10] C. Clark. *Aircraft noise effects on health*. Tech. rep. Prepared for the Airports Commission. Queen Mary University of London, May 2015. URL: https://assets.publishing.service.gov.uk/government/uploads/system/uploads/attachment_data/file/446311/noise-aircraft-noise-effects-on-health.pdf (cit. on p. 3).

[11] A. W. Correia, J. L. Peters, J. I. Levy, and S. Melly. *Residential exposure to aircraft noise and hospital admissions for cardiovascular diseases: multi-airport retrospective study*. Tech. rep. BMJ 2013;347:f5561. Oct. 2013 (cit. on p. 3).

[12] Nick Cumpsty, Dimitri Mavris, and Michelle Kirby. *Aviation and the Environment: Outlook*. Environmental Report. ICAO, 2019, pp. 24–38. URL: https://www.icao.int/environmental-protection/Documents/EnvironmentalReports/2019/ENVReport2019_pg24-38.pdf (cit. on pp. 4, 5).

[13] D. G. Dunn and N. A. Peart. *Aircraft Noise Source and Contour Estimation*. Contractor Report (CR) NASA-CR-114649. Boeing Commercial Airplane Co. Seattle, WA, United States: NASA, 1973 (cit. on pp. 21, 22, 25).

[14] L. Ellbrant and D. Karlson. "A Noise Prediction Tool for Subsonic Aircraft and Engines including a Numerical Investigation of Noise Radiation". MA thesis. Gothenburg, Sweden: Chalmers University of Technology, 2008 (cit. on p. 8).

[15] T. Elliff, M. Cremaschi, and V. Huck. *Impact of aircraft noise pollution on residents of large cities*. Tech. rep. PE 650.787. Brussels: Policy Department for Citizens' Rights and Constitutional Affairs, European Parliament, Jan. 2021. URL: https://www.europarl.europa.eu/RegData/etudes/STUD/2020/650787/IPOL_STU(2020)650787_EN.pdf (cit. on p. 3).

[16] Eurocontrol. *Charting the European Aviation recovery: 2021 COVID19 impacts and 2022 outlook*. Jan. 2022. URL: https://www.eurocontrol.int/sites/default/files/2022-01/eurocontrol-think-paper-15-2021-review-2022-outlook_0.pdf (visited on 04/27/2022) (cit. on p. 3).

[17] European Civil Aviation Conference (ECAC). *Report on Standard Method of Computing Noise Contours around Civil Airports, 4th Edition*. Tech. rep. Neuilly-sur-Seine Cédex, France: European Civil Aviation Conference, Dec. 2016. URL: https://www.ecac-ceac.org/images/documents/ECAC-Doc_29_4th_edition_Dec_2016_Volume_3_Part_1.pdf (cit. on p. 6).

[18] European Union Aviation Safety Agency, European Environment Agency, and Eurocontrol. *European Aviation Environmental Report 2019*. Tech. rep. European Union Aviaion Safety Agency (EASA), May 2019. URL: https://www.easa.europa.eu/eaer/system/files/usr_uploaded/219473_EASA_EAER_2019_WEB_HI-RES_190311.pdf (cit. on p. 3).

[19] Federal Aviation Administration (FAA). *Aviation Environmental Design Tool (AEDT) Version 3d*. URL: https://aedt.faa.gov/3d_information.aspx (visited on 04/27/2022) (cit. on p. 6).

[20] A. Filippone. "Aircraft noise prediction". In: *Progress in Aerospace Sciences* 68 (Mar. 2014), pp. 27–63. DOI: 10.1016/j.paerosci.2014.02.001 (cit. on p. 7).

[21] P. Gliebe, R. Mani, H. Shin, B. Mitchell, G. Ashford, S. Salamah, and S. Connell. *Aeroacoustic Prediction Codes*. Contractor Report NASA/CR-2000-210244. Glenn Research Center: NASA, 2000 (cit. on pp. 18, 21).

[22] Philip R. Gliebe and Bangalore A. Janardan. *Ultra-High Bypass Engine Aeroacoustic Study*. Technical Report NASA/CR-2003-212525, E-14087. Cincinnati, OH, United States: General Electric Aircraft Engines, Oct. 2003 (cit. on p. 4).

[23] Robert A. Golub, Rahul Sen, Bruce Hardy, Kingo Yamamoto, Yue-Ping Guo, and Gregory Miller. *Airframe Noise Sub-Component Definition and Model*. Contractor Report (CR) NASA/CR-2004-213255. Langley Research Center, Hampton, Virginia: NASA, 2004 (cit. on p. 24).

[24] Justin S. Gray, John T. Hwang, Joaquim R. R. A. Martins, Kenneth T. Moore, and Bret A. Naylor. "OpenMDAO: an open-source framework for multidisciplinary design, analysis, and optimization". In: *Structural and Multidisciplinary Optimization* 59 (2019), pp. 1075–1104 (cit. on p. 31).

[25] J. E. Green. "Greener by Design — the technology challenge". In: *The Aeronautical Journal* 106.1056 (Feb. 2002), pp. 57–113. DOI: 10.1017/S0001924000095993 (cit. on p. 31).

[26] J. F. Groeneweg and E. J. Rice. "Aircraft Turbofan Noise". In: *Journal of Turbomachinery* 109.1 (Jan. 1987), pp. 130–141. DOI: 10.1115/1.3262058 (cit. on p. 25).

[27] Tomas Grönstedt. "Development of methods for analysis and optimization of complex jet engine systems". Ph.D. Thesis. Gothenburg, Sweden: Chalmers University of Technology, 2000 (cit. on p. 8).

[28] Tomas Grönstedt, Dax Au, Konstantinos G. Kyprianidis, and Stephen Ogaji. "Low-Pressure System Component Advancements and Its Influence on Future Turbofan Engine Emissions". In: *Proceedings of ASME Turbo Expo 2009: Power for Land, Sea and Air*. Orlando, Florida, USA, June 2009. DOI: 10.1115/GT2009-60201 (cit. on p. 8).

[29] Y. Guo. *Empirical Prediction of Aircraft Landing Gear Noise*. Contractor Report NASA/CR-2005-213780. VA, United States: NASA Langley Research Center Hampton, July 2005. URL: https://ntrs.nasa.gov/citations/20050209966 (cit. on p. 24).

[30] Marcus F. Heidmann. *Interim Prediction Method for Fan and Compressor Source Noise*. Technical Memorandum (TM) NASA-TM-X-71763. Lewis Research Center, Cleveland, Ohio: NASA, June 1979 (cit. on pp. 17, 18).

[31] A. S. Hersh, F. W. Burcham Jr., T. W. Putnam, and P. L. Lasagna. *Semiempirical Airframe Noise Prediction Model and Evaluation with Flight Data*. Technical Memorandum NASA TM X-56041. CA, United States: NASA Hugh L. Dryden Flight Research Center, Dec. 1976. URL: https://ntrs.nasa.gov/citations/19770006848 (cit. on p. 23).

[32] International Civil Aviation Organization (ICAO). *Aircraft Noise*. URL: https://www.icao.int/environmental-protection/pages/noise.aspx (visited on 04/27/2022) (cit. on p. 3).

[33] International Civil Aviation Organization (ICAO). *Continuous Descent Operations (CDO) Manual*. Tech. rep. Doc 9931, AN/476. International Civil Aviation Organization (ICAO), 2010. URL: https://applications.icao.int/tools/ATMiKIT/story_content/external_files/102600063919931_en.pdf (visited on 04/27/2022) (cit. on p. 5).

[34] International Civil Aviation Organization (ICAO). *Procedures for Air Navigation Services - Aircraft Operations (PANS-OPS): Part I*. Tech. rep. Doc 8168, OPS/611. International Civil Aviation Organization (ICAO), Nov. 2006. URL: http://www.chcheli.com/sites/default/files/icao_doc_8168_vol_1.pdf (cit. on p. 5).

[35] K. Jones. *Aircraft Noise and Children's Learning*. Tech. rep. ERCD REPORT 0908. London: Civil Aviation Authority (CAA), Feb. 2010. URL: https://publicapps.caa.co.uk/docs/33/ERCD200908.pdf (cit. on p. 3).

[36] K. Jones. *Aircraft noise, sleep disturbance and health effects*. Tech. rep. CAP 1164. London: Civil Aviation Authority (CAA), 2014. URL: https://publicapps.caa.co.uk/docs/33/CAP%201164_Aircraft%20noise_and_health.pdf (cit. on p. 3).

[37] K. Knobloch et al. "Future Aircraft and the Future of Aircraft Noise". In: *Aviation Noise Impact Management*. Cham, Switzerland: Springer, Jan. 2022, pp. 117–139. ISBN: 978-3-030-91193-5 (cit. on p. 4).

[38] R. Koenig and O. Macke. "Evaluation of simulator and flight tested noise abatement approach procedures". In: *ICAS 2008-4.8.1*. Anchorage, Alaska, USA, Sept. 2008 (cit. on p. 6).

[39] K. B. Kontos, B. A. Janardan, and P. R. Gliebe. *Improved NASA-ANOPP Noise Prediction Computer Code for Advanced Subsonic Propulsion Systems*. Contractor Report 195480. Cincinnati, OH United States: NASA Lewis Research Center, Aug. 1996. URL: https://ntrs.nasa.gov/citations/19960048499 (cit. on pp. 17, 18).

[40] E. A. Krejsa and J. R. Stone. *Enhanced Fan Noise Modeling for Turbofan Engines*. Contractor Report NASA/CR—2014-218421. Cincinnati, OH, United States: Diversitech, Inc., Dec. 2014. URL: https://ntrs.nasa.gov/citations/20150000884 (cit. on p. 25).

[41] E. A. Krejsa and M. F. Valerino. *Interim prediction method for turbine noise*. Technical Memorandum NASA-TM-X-73566. Cleveland, OH, United States: NASA Lewis Research Center, Nov. 1976. URL: https://ntrs.nasa.gov/citations/19770006122 (cit. on p. 25).

[42] P. L. Lasagna, K. G. Mackall, F. W. Burcham Jr., and T. W. Putnam. *Landing Approach Airframe Noise Measurements and Analysis*. Technical Publication NASA-TP-1602. CA, United States: NASA Hugh L. Dryden Flight Research Center Edwards, Jan. 1980. URL: https://ntrs.nasa.gov/citations/19800006769 (cit. on p. 24).

[43] L. Leylekian, M. Lebrun, and P. Lempereur. "An overview of aircraft noise reduction technologies". In: *Aerospace Lab, Alain Appriou* 7 (June 2014), pp. 1–15. DOI: 10.12762/2014.AL07-01 (cit. on p. 25).

[44] X. Liu, D. Zhao, D. Guan, S. Becker, D. Sun, and X. Sun. "Development and progress in aeroacoustic noise reduction on turbofan aeroengines". In: *Progress in Aerospace Sciences* 130 (Apr. 2022). DOI: 10.1016/j.paerosci.2021.100796 (cit. on p. 4).

[45] A. Miele. *Flight Mechanics: Theory of Flight Paths*. Dover Books on Aeronautical Engineering. Mineola, New York: Dover Publications, Inc., Apr. 2016. ISBN: 9780486801469 (cit. on pp. 11, 12).

[46] *Novair*. URL: https://www.novair.se/ (visited on 01/04/2021) (cit. on p. 8).

[47] D. P. Raymer. *Aircraft Design: A Conceptual Approach, Sixth Edition*. Playa del Ray, CA, United State: American Institute of Aeronautics Astronautics, 2018 (cit. on p. 24).

[48] J. W. Russel. *An empirical method for predicting the mixing noise levels of subsonic circular and coaxial jets*. Contractor Report (CR) NASA-CR-3786. Langley Research Center, Hampton, VA, United States: NASA, 1984 (cit. on pp. 22, 23).

[49] SAE Aerospace. *Method for Predicting Lateral Attenuation of Airplane Noise*. Aerospace Information Report SAE AIR 5662 Rev. D. SAE International, Apr. 2006 (cit. on p. 26).

[50] SAE Aerospace. *Standard Values Of Atmospheric Absorption As A Function Of Temperature And Humidity*. Tech. rep. SAE ARP866A-1975. Feb. 1975 (cit. on p. 28).

[51] *SAFT*. Feb. 2022. URL: https://www.kth.se/csa/projekt/avslutade-projekt/saft-1.991973 (visited on 04/27/2022) (cit. on pp. 8, 32).

[52] SkyVector. *ESSA Stockholm Arlanda Airport*. URL: https://skyvector.com/airport/ESSA/Stockholm-Arlanda-Airport (visited on 05/02/2022) (cit. on p. 15).

[53] V. Sparrow et al. *Aviation Noise Impacts White Paper*. Environmental Report. ICAO, 2019, pp. 44–61. URL: https://www.icao.int/environmental-protection/Documents/ScientificUnderstanding/EnvReport2019-WhitePaper-Noise.pdf (cit. on p. 3).

[54] U. Tengzelius and A. Johansson. *Aircraft noise mapping code SAFT*. Tech. rep. Stockholm, Sweden: Centre of Sustainable Aviation (CSA), 2021. URL: https://docs.google.com/document/d/1OhJqkSLCMbYAqSwZzUtK1rZXEuKq-0t1lsiLvkwUIRg/edit (cit. on p. 28).

[55] *ULLA*. Feb. 2021. URL: https://www.kth.se/en/csa/projekt/ulla-1.979419 (visited on 04/27/2022) (cit. on p. 8).

[56] C. Veness. *Calculate distance, bearing and more between Latitude/Longitude points*. URL: https://www.movable-type.co.uk/scripts/latlong.html (visited on 05/02/2022) (cit. on pp. 14, 15).

[57] H. G. Visser and R. A. A. Wijnen. "Optimization of Noise Abatement Departure Trajectories". In: *Journal of Aircraft* 38.4 (July 2001), pp. 620–627. DOI: 10.2514/2.2838 (cit. on p. 6).

[58] W. L. Willshire Jr. and D. P. Garber. *Advanced Subsonic Transport Approach Noise: The Relative Contribution of Airframe Noise*. Technical Memorandum NASA-TM-104112. Hampton, VA, United States: NASA Langley Research Center, June 1992. URL: https://ntrs.nasa.gov/citations/19920024904 (cit. on p. 26).

[59] M. R. Wilson. *An introduction to high speed aircraft noise prediction*. Contractor Report NASA-CR-189582. Hampton, VA, United States: Lockheed Engineering and Sciences Co., Feb. 1992. URL: https://ntrs.nasa.gov/citations/19920010430 (cit. on p. 25).

[60] L. Yong, W. Xunnian, and Z. Dejiu. "Control strategies for aircraft airframe noise reduction". In: *Chinese Journal of Aeronautics* 26.2 (Apr. 2013), pp. 249–260. DOI: 10.1016/j.cja.2013.02.001 (cit. on p. 5).

[61] C. Zellmann, B. Schäffer, J. M. Wunderli, U. Isermann, and C. O. Paschereit. "Aircraft Noise Emission Model Accounting for Aircraft Flight Parameters". In: *Journal of Aircraft* 55.2 (Aug. 2017). DOI: 10.2514/1.C034275 (cit. on p. 7).

[62] M. Zhang and A. Filippone. "Optimum problems in environmental emissions of aircraft arrivals". In: *Aerospace Science and Technology* 123 (Apr. 2022). DOI: 10.1016/j.ast.2022.107502 (cit. on p. 6).

[63] M. Zhang, A. Filippone, and N. Bojdo. "Multi-objective optimisation of aircraft departure trajectories". In: *Aerospace Science and Technology* 79 (Aug. 2018), pp. 37–47. DOI: 10.1016/j.ast.2018.05.032 (cit. on p. 6).

[64] W. E. Zorumski. *Aircraft noise prediction program theoretical manual, Parts 1 and 2*. Technical Memorandum 83199. Hampton, VA, United States: NASA, Feb. 1982. URL: https://ntrs.nasa.gov/citations/19820012072 (cit. on pp. 7, 27).